

## The Ginninderra CH<sub>4</sub> and CO<sub>2</sub> release experiment: An evaluation of gas detection and quantification techniques

Andrew Feitz<sup>a,b,\*</sup>, Ivan Schroder<sup>a,b</sup>, Frances Phillips<sup>c</sup>, Trevor Coates<sup>d</sup>, Karita Negandhi<sup>e</sup>, Stuart Day<sup>f</sup>, Ashok Luhar<sup>g</sup>, Sangeeta Bhatia<sup>h</sup>, Grant Edwards<sup>e</sup>, Stefan Hrabar<sup>i</sup>, Emili Hernandez<sup>i</sup>, Brett Wood<sup>i</sup>, Travis Naylor<sup>c</sup>, Martin Kennedy<sup>e</sup>, Murray Hamilton<sup>j</sup>, Mike Hatch<sup>j</sup>, John Malos<sup>k</sup>, Mark Kochanek<sup>k</sup>, Peter Reid<sup>k</sup>, Joel Wilson<sup>c</sup>, Nicholas Deutscher<sup>c</sup>, Steve Zegelin<sup>l</sup>, Robert Vincent<sup>j</sup>, Stephen White<sup>f</sup>, Cindy Ong<sup>m</sup>, Suman George<sup>n,o</sup>, Peter Maas<sup>p</sup>, Sean Towner<sup>q</sup>, Nicholas Wokker<sup>r</sup>, David Griffith<sup>c</sup>

<sup>a</sup> Geoscience Australia, Canberra, Australia

<sup>b</sup> CO2CRC, Melbourne, Australia

<sup>c</sup> University of Wollongong, Wollongong, Australia

<sup>d</sup> University of Melbourne, Melbourne, Australia

<sup>e</sup> Macquarie University, Sydney, Australia

<sup>f</sup> CSIRO Energy, Newcastle, Australia

<sup>g</sup> CSIRO Oceans and Atmosphere, Aspendale, Australia

<sup>h</sup> Western Sydney University, Parramatta, Australia

<sup>i</sup> CSIRO Data 61, Pullenvale, Australia

<sup>j</sup> University of Adelaide, Adelaide, Australia

<sup>k</sup> CSIRO Energy, Pullenvale, Australia

<sup>l</sup> CSIRO Oceans and Atmosphere, Canberra, Australia

<sup>m</sup> CSIRO Mineral Resources, Melbourne, Australia

<sup>n</sup> University of Western Australia, Perth, Australia

<sup>o</sup> National Geosequestration Laboratory, Perth, Australia

<sup>p</sup> Bruker Optik GmbH, Ettlingen, Germany

<sup>q</sup> FLIR Systems Australia Pty Ltd, Baulkham Hills, Australia

<sup>r</sup> Department of Industry, Innovation and Science, Canberra, Australia

### ARTICLE INFO

#### Keywords:

Fugitive emissions  
Methane  
Carbon dioxide  
Geological storage  
Geosequestration  
Quantification  
Measurement  
Modelling  
Atmospheric  
Leakage

### ABSTRACT

A methane (CH<sub>4</sub>) and carbon dioxide (CO<sub>2</sub>) release experiment was held from April to June 2015 at the Ginninderra Controlled Release Facility in Canberra, Australia. The experiment provided an opportunity to compare different emission quantification techniques against a simulated CH<sub>4</sub> and CO<sub>2</sub> point source release, where the actual release rates were unknown to the participants. Eight quantification techniques were assessed: three tracer ratio techniques (two mobile); backwards Lagrangian stochastic modelling; forwards Lagrangian stochastic modelling; Lagrangian stochastic (LS) footprint modelling; atmospheric tomography using point and using integrated line sensors. The majority of CH<sub>4</sub> estimates were within 20% of the actual CH<sub>4</sub> release rate (5.8 g/min), with the tracer ratio technique providing the closest estimate to both the CH<sub>4</sub> and CO<sub>2</sub> release rates (100 g/min). Once the release rate was known, the majority of revised estimates were within 10% of the actual release rate. The study illustrates the power of measuring the emission rate using multiple simultaneous methods and obtaining an ensemble median or mean. An ensemble approach to estimating the CH<sub>4</sub> emission rate proved successful with the ensemble median estimate within 16% for the actual release rate for the blind release experiment and within 2% once the release rate was known. The release also provided an opportunity to assess the effectiveness of stationary and mobile ground and aerial CH<sub>4</sub> detection technologies. Sensor detection limits and sampling rates were found to be significant limitations for CH<sub>4</sub> and CO<sub>2</sub> detection. A hyperspectral imager's capacity to image the CH<sub>4</sub> release from 100 m, and a Boreal CH<sub>4</sub> laser sensor's ability to track moving targets suggest the future possibility to map gas plumes using a single laser and mobile aerial reflector.

\* Corresponding author at: Geoscience Australia, Canberra, Australia.

E-mail address: [andrew.feitz@ga.gov.au](mailto:andrew.feitz@ga.gov.au) (A. Feitz).

<https://doi.org/10.1016/j.ijggc.2017.11.018>

Received 4 August 2017; Received in revised form 14 November 2017; Accepted 18 November 2017

Available online 15 March 2018

1750-5836/ Crown Copyright © 2017 Published by Elsevier Ltd. This is an open access article under the CC BY license (<http://creativecommons.org/licenses/by/4.0/>).

### 1. Introduction

Reducing emissions from the extraction, transportation, and burning of fossil fuels is an important mechanism for many countries in order to limit their greenhouse gas emissions by 2030 and thereby reduce the impacts of climate change (UNFCCC, 2015). Verification of reduction in emissions, especially fugitive methane (CH<sub>4</sub>) emissions, will become increasingly important to assess the effectiveness of low emissions technologies and greenhouse gas reduction strategies. Fugitive CH<sub>4</sub> emissions occur during the mining of coal, the production of conventional gas, and extraction of unconventional gas extracted from coal seams or shales, and its further processing, storage and transportation. The blowout of a well connected to the Aliso Canyon underground natural gas storage facility in California during 2015 resulted in a massive release of CH<sub>4</sub>, where atmospheric leak rates of up to 60 metric tonnes of CH<sub>4</sub> per hour were estimated (Conley et al., 2016). This underscores the importance of identifying and quantifying fugitive emissions. Atmospheric monitoring technologies are an ideal method for investigating fugitive emissions (Jenkins et al., 2012; Zazzeri et al., 2015; Omara et al., 2016) and have been used to estimate emission rates from natural CO<sub>2</sub> seepage sites (Werner et al., 2003; Lewicki et al., 2008; Jones et al., 2009). They are likely to play an increasingly important role in the verification of claimed greenhouse emission reductions and quantification of leakage events. High confidence in the accuracy of the quantification methods employed is therefore essential and is a legislative requirement of various governments (Dixon and Romanak, 2015).

There have been a number of recent attempts using controlled

release experiments to improve atmospheric techniques for quantifying greenhouse gas emissions, which could be applied to the fossil fuel resources sector and geological storage projects (Loh et al., 2009; Lewicki and Hillel, 2009; Humphries et al., 2012; Kuske et al., 2013; Etheridge et al., 2011; Jenkins et al., 2016; Luhar et al., 2014; van Leeuwin et al., 2013; Ro et al., 2011; Hirst et al., 2017). For example, CO<sub>2</sub> and CH<sub>4</sub> atmospheric detection and quantification techniques for have been previously assessed at the CO2CRC Otway site in Victoria, Australia in 2011. Here CO<sub>2</sub> (8 t/d) and CH<sub>4</sub> (730 kg/d) were released intermittently over 1 month at a height of 2.5 m above the ground. Identification of the source gas location was accomplished by the atmospheric tomography technique using an array of solar powered CO<sub>2</sub> sensors (Kuske et al., 2013; Jenkins et al., 2016). For quantification, a Bayesian inverse atmospheric model coupled to a backward Lagrangian particle dispersion model with a Markov Chain Monte Carlo method for sampling the posterior probability proved to be effective to quantify CH<sub>4</sub> emissions. However, it was less successful with the CO<sub>2</sub> emissions due to the lower signal-to-noise ratio (Luhar et al., 2014).

Supporting the advancements obtained from controlled release experiments is the Ginninderra greenhouse gas controlled release facility in Canberra, Australia. This facility was designed to evaluate the effectiveness of different near surface monitoring techniques for detecting and quantifying leaks against a known gas source. Experiments conducted to date include an above ground CO<sub>2</sub> and N<sub>2</sub>O release experiment in 2010 (Humphries et al., 2012) and three sub-surface CO<sub>2</sub> release experiments conducted from 2012 to 2013, releasing between 144 and 218 kg of CO<sub>2</sub> per day (Feitz et al., 2014a, 2016). Together, these previous experiments have brought a strong focus at the Ginninderra

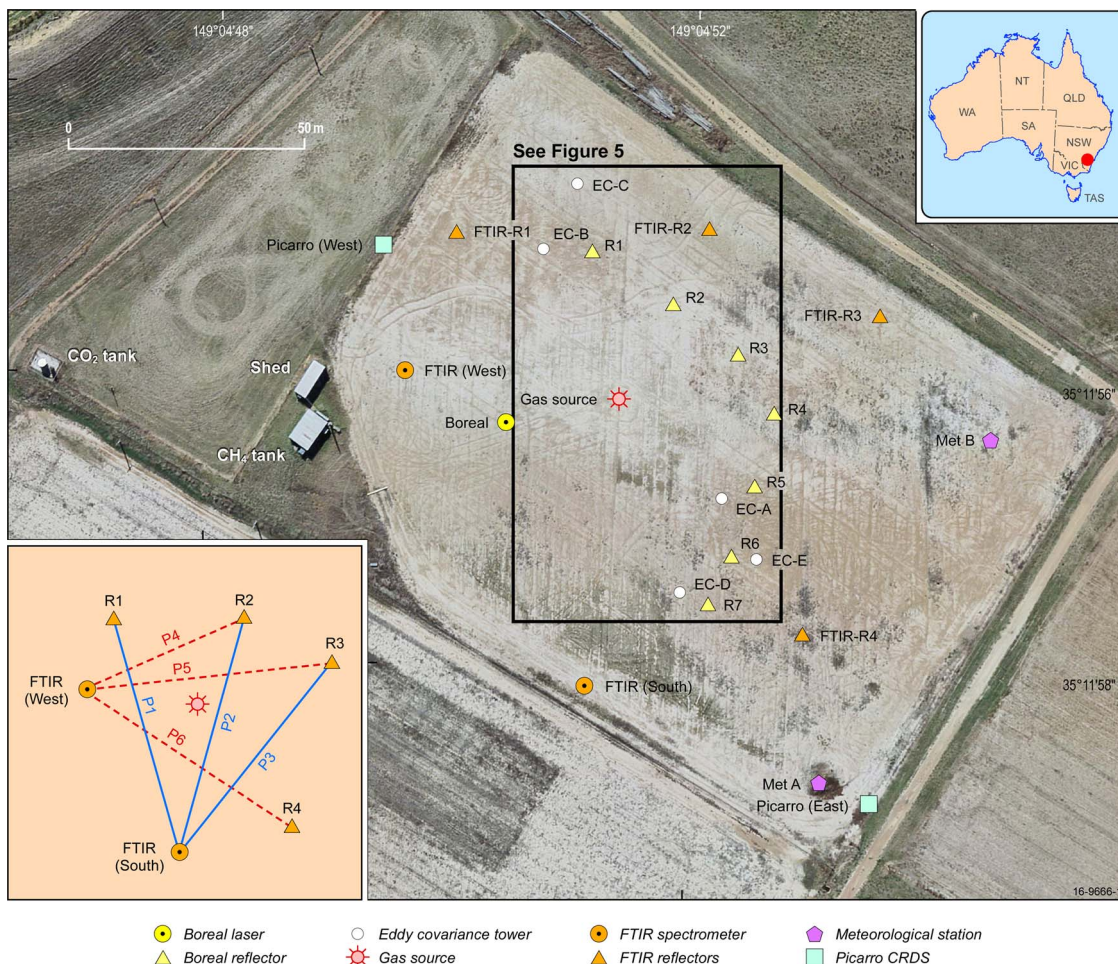


Fig. 1. Location of equipment deployed at the Ginninderra controlled release facility for the methane release experiment and with numbering for FTIR paths indicated in the insert.

site to evaluate the effectiveness of atmospheric monitoring techniques for quantification of emissions.

In April–July 2015, a blind release experiment with a combined CO<sub>2</sub> and CH<sub>4</sub> point source was conducted at Ginninderra. The primary objectives of the experiment were to 1) evaluate an array of eight stationary and mobile CH<sub>4</sub> detection technologies and 2) to conduct a comparison of different emissions quantification techniques against a CO<sub>2</sub> and CH<sub>4</sub> controlled release. This was achieved through assessing eight quantification techniques: three tracer ratio techniques (two mobile); backwards Lagrangian stochastic modelling; forwards Lagrangian stochastic modelling; Lagrangian stochastic (LS) footprint modelling; atmospheric tomography using point sensors; and atmospheric tomography using integrated line sensors. The Gaussian, Lagrangian and footprint techniques used to describe atmospheric dispersion in this study are all well-established, classical techniques in atmospheric science. The novelty in this study is the comprehensive inter-comparison between the different quantification methods, coupling them to new instrumentation platforms and, in some cases, undertaking inversions and incorporating Bayesian statistics. The quantification component of this study also assumes that the location of a leak or multiple leaks is known and has been previously identified, attributed and mapped using other monitoring techniques. This enables optimum placement of instrumentation for quantifying leakage (e.g. upwind/downwind of the leak).

## 2. Methods

### 2.1. Field site

The Ginninderra greenhouse gas controlled release facility was designed and developed under a joint venture between the Cooperative Research Centre for Greenhouse Gas Technologies (CO2CRC) and Geoscience Australia, with CSIRO hosting the site at its Ginninderra Experimental Station in north Canberra. The facility was designed to simulate surface emissions of CO<sub>2</sub> and other greenhouse gases from the soil into the atmosphere. The experiment, including baseline data collection, spanned from 23 April to 23 June 2015. The site, shown in Fig. 1, was a flat, fallow field surrounded by fields used for sheep grazing and cropping. A 6 m high earth-fill dam wall was 120 m north-west of the release point. A shed housing the instrumentation was located approximately 60 m west of the release point. The average temperature during the two-month campaign was 7.7 °C (range –4.8 °C to 22.3 °C) and during the autumn-winter season the wind was dominated by north westerlies.

### 2.2. Emission sources

Mass flow controllers (MFCs) were used to meter the simultaneous release of CO<sub>2</sub>, N<sub>2</sub>O and CH<sub>4</sub> for the duration of the experiment. A summary of the release rates during the experiment is given in Table 1. Scientific grade CO<sub>2</sub> was supplied from a 2.5 t on-site liquid CO<sub>2</sub> tank, via a vaporiser, with the gas flow controlled using Burkert 8626 MFCs. The metered CO<sub>2</sub> flow was then distributed to the release chamber using 10 mm Dekabon® tubing to a 0.30 m diameter mixing (release) chamber, 0.30 m above ground. The chamber was perforated on the underside to enable even distribution of the released gas. A pair of cylinders of high purity CH<sub>4</sub> gas, each about 7.5 m<sup>3</sup> at STP, supplied the CH<sub>4</sub> flow, with another pair connected to the manifold for easy swap over. CH<sub>4</sub> flow was metered with a gas-specific and calibrated Sierra Smart-Trak MFC and distributed to the release chamber via ¼ inch polyurethane tubing. N<sub>2</sub>O was used as a tracer in the experiment. It was metered using a gas-specific and calibrated Sierra Smart-Trak MFC and mixed with the metered CO<sub>2</sub> in a stainless steel mixing chamber prior to distribution via ¼ inch polyurethane tubing to the release chamber. Acetylene (C<sub>2</sub>H<sub>2</sub>) was released also on three days (25–27 May 2015) as a tracer and metered using a gas-specific and calibrated Sierra Smart-

Trak MFC via ¼ inch polyurethane tubing. The standard C<sub>2</sub>H<sub>2</sub> release rate was 1.4 g/min.

### 2.3. Field instrumentation

#### 2.3.1. Picarro CRDS analysers

Two “fixed” Picarro G2201-i gas analysers were deployed at the site from 21 May to 23 June (Fig. 1) by CSIRO and Geoscience Australia. The “West Picarro” was located inside the shed and its inlet was supplied via a separate offtake line from a Thomas air pump. The pump was used to draw air along an approximately 40 m length of Dekabon® tubing from a 2 m tall intake located NNE of the shed. This instrument ran without interruption during its deployment. A second G2201-i Picarro (“East Picarro”) was installed in the far south-eastern corner of the field. This instrument was completely powered using 4 × 125 W solar panels with six 2 V × 1750 AH batteries. The low solar irradiation during the autumn/winter conditions meant that there was insufficient power to operate the instrument continuously during the experiment; hence the instrument was often powered down overnight or could be offline for up to 3 days. Despite both instruments being calibrated for both isotopic and concentration measurements of CO<sub>2</sub> and CH<sub>4</sub> immediately prior to deployment, there was low confidence in the isotopic readings taken and only the concentration values are used in this paper.

#### 2.3.2. Boreal GasFinder2 laser

A scanning Boreal GasFinder2 open path tuneable diode laser (TDL) was deployed for the experiment by Geoscience Australia from 27 April to 12 June. It was equipped with an automated scanning mount, powered using 240 V mains power, and was located approximately 25 m west of the release chamber. Seven laser paths were set up at a height of approximately 1.5 m. The reflectors for each path were positioned in a semi-circle around the release chamber, with the lengths of the paths ranging from 40 m to 57 m (Fig. 1). Each reflector comprised an array of 9 gold corner retro-reflectors. The laser polled a reflector every 2 s and then cycled through the reflectors in intervals of 20 s.

#### 2.3.3. Eddy covariance towers

Five eddy covariance towers were used during the release experiment and their layout is shown in Fig. 1. All towers collected data at a frequency of 10 Hz and their configuration in the field is summarised in Table 2 below. A full description of the eddy covariance method can be found in Baldocchi (2003).

Tower A (CSIRO) comprised a Vaisala HMP50 RH and temperature sensor, a CSI CSAT3 sonic anemometer, a CSI EC150 CO<sub>2</sub>-H<sub>2</sub>O sensor, a Li-COR 7700 CH<sub>4</sub> sensor, a Kipp and Zonen CNR4 radiometer, and a Gill WindSonic 2D sonic anemometer. Tower B (University of Western Australia) comprised a Vaisala HMP50 RH and temperature sensor, a CSI CSAT3 sonic anemometer, a Li-COR 7700 CH<sub>4</sub> sensor, a Kipp and Zonen CNR4 radiometer, and a Gill WindSonic 2D sonic anemometer. Towers C and D (University of Adelaide/Macquarie University) were equipped with a Gill WindSonic 3D sonic anemometer, a Li-COR 7700 CH<sub>4</sub> sensor, and Li-COR 7550 SmartFlux data system. Tower C is in the predominant upwind position from the emission source, while Tower D

**Table 1**

Emission rates during the 2015 release experiment. Releases limited to daytime only except for the evenings of 17, 18, 21 and 28 May and 5 and 6 June. The standard CH<sub>4</sub> release rate of 5.8 g/min is equivalent to an emission rate of 8.4 kg/d CH<sub>4</sub> and 300 g/min for CO<sub>2</sub> is equivalent to 0.43 t/d.

Period	CH <sub>4</sub> g/min	CO <sub>2</sub> g/min	N <sub>2</sub> O g/min
23 April–25 May	5.8 (standard rate)	50	1.1
26 May–27 May	0–20	100	1.1
25 May–7 June	5.8 (standard rate)	100	1.1
8 June–12 June	5.0	300	1.1
23 June–24 June	0–20	0	0

**Table 2**  
Summary of eddy covariance tower configurations.

	Measurement Height (m)	Distance from source (m)	Bearing	Measurement dates
Tower A	2.30	30	134°	5 May–22 June
Tower B	2.27	35	334°	24 April–22 June
Tower C	3.03	43	346°	16 May–5 June
Tower D	3.03	46	153°	16 May–5 June
Tower E	4.7	45	140°	24 April–8 June

is in the predominant downwind (D) position. Tower E (University of Melbourne) was equipped with an identical instrument suite to towers C and D.

#### 2.3.4. Hyperspectral imager

A Bruker hyperspectral imager (HI90) was deployed from 26 to 27 May by Bruker Optik. The passive imaging Fourier transform infrared spectroscopy (FTIR) instrument is based on the combination of a Michelson interferometer and a  $256 \times 256$  pixels focal plane array (FPA) infrared detector. The sensor package contains an internal calibration source, a video camera and a Global Positioning (GPS) receiver. In operation, the HI90 is mounted on a pan and tilt head which can then be controlled by software to provide a  $360^\circ$  field of view. The instrument that was used for the trial operated in the  $870\text{--}1440\text{ cm}^{-1}$  spectral range at a spectral resolution of  $4\text{ cm}^{-1}$  and  $0.7\text{ cm}^{-1}$ . The spatial (pixel) resolution and the spectral resolution were continuously tested to optimise the detection limit but for the majority of the trial Images  $128 \times 128$  pixel resolution and  $4\text{ cm}^{-1}$  spectral resolution (single scans, 700 ms scan time) were used.

#### 2.3.5. Open path FTIR

A full description of the OP-FTIR instrument is given in the Supplementary data M1. Briefly, the instrument consists of an FTIR spectrometer, (Matrix IR-Cube, Bruker Optik GmbH, Ettlingen, Germany) equipped with a mechanically cooled ( $-196^\circ\text{C}$ , RicorK508) MCT detector (Infrared Associates Inc., Florida, USA, or Judson Industries, Montgomeryville, PA, USA) coupled to a 250 mm Schmidt-Cassegrain telescope (LX 200ACF, Meade Instruments Corporation, Irvine California, USA) modified to act as a beam expander. The system is mounted on a computer controlled automated instrument mount

(AIM, Illawarra Automation and Control; Unanderra, Australia) to allow automated alignment of the beam between spectrometer and multiple retro-reflectors, with the system providing path-averaged concentrations of  $\text{NH}_3$ ,  $\text{N}_2\text{O}$ ,  $\text{CO}_2$ ,  $\text{CH}_4$ ,  $\text{CO}$  and water vapour (Griffith, 1996) over the open atmospheric path between spectrometer and retro-reflector located 50–500 m from the instrument.

Two OP-FTIR systems were deployed by the University of Wollongong, with 4 retro-reflectors terminating 6 paths, 3 paths for each instrument (Fig. 1). Each instrument rotated between the three paths on a 5 min cycle. The mixing-ratio data for each path were calibrated, based on data collected when wind speeds was  $>2\text{ m/s}$  and gas was not being released. The calibrated data for each path were averaged to 30 min and synchronised to the meteorological data.

Data were collected between 4 May and 12 June. Generally data collection was halted when gas was not released, with the instruments operated for extended hours to collect data without a source gas for calibration purposes occasionally when predicted meteorological conditions were favourable. Initially meteorological data were obtained from EC Tower A and subsequently from the University of Wollongong weather station following installation on 16 May (see Supplementary data M1 for details).

#### 2.3.6. Mobile Los Gatos Research cavity enhanced spectroscopy $\text{CH}_4/\text{C}_2\text{H}_2/\text{H}_2\text{O}$ analyser

For the  $\text{C}_2\text{H}_2$  tracer gas experiments, a Los Gatos Research  $\text{CH}_4/\text{C}_2\text{H}_2/\text{H}_2\text{O}$  Ultraportable Analyser (LGR) was used by CSIRO to measure downwind concentrations of both  $\text{CH}_4$  and  $\text{C}_2\text{H}_2$  from 26 to 27 May. This instrument has a nominal operating range of 0–1000 ppm  $\text{CH}_4$  and  $\text{C}_2\text{H}_2$  with a precision of less than 1 ppb and is battery powered so that it can be used in the field. During these experiments, the analyser was mounted on a trolley so that it could be moved through the gas plume at distances ranging from a few meters to about 200 m from the gas release point. The inlet to the instrument was approximately 1 m above ground level during all of the tracer experiments. A GPS receiver (Hemisphere R3300 GNSS Receiver) provided the location of the analyser within the field during each experiment. The calibration of the analyser was checked against several standard gas mixtures including a high precision reference air sample containing 1.732 ppm  $\text{CH}_4$  prepared by the CSIRO Oceans and Atmosphere, GASLAB (Francey et al., 2003). Two other commercially prepared standards (BOC Australia) containing 7.0 ppm  $\text{CH}_4$  and 4.1 ppm  $\text{C}_2\text{H}_2$ , and 21.6 ppm  $\text{CH}_4$  and 20.6 ppm  $\text{C}_2\text{H}_2$ ,

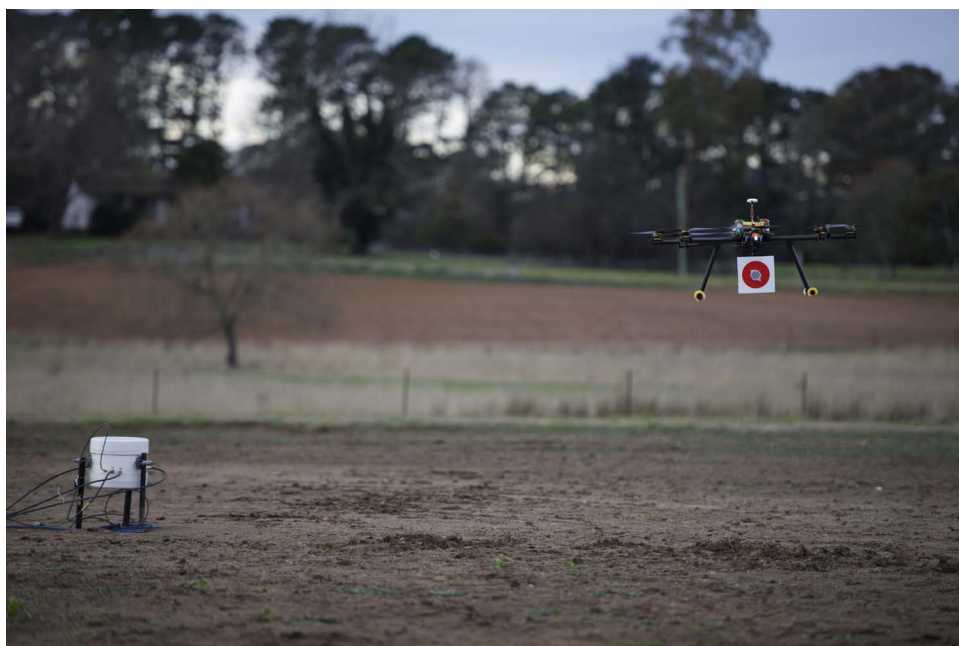


**Fig. 2.** Boreal GasFinder2 UAV octocopter target with reflector payload near the gas release chamber.

respectively were also used and demonstrated the sensor was performing optimally.

### 2.3.7. Zebgas

The Zebgas sensing unit was developed by CSIRO using lightweight CO<sub>2</sub> and CH<sub>4</sub> sensors to allow easy integration into the handheld Zebdee scanner (Bosse et al., 2012) or attached as a slung payload to an Unmanned Aerial Vehicle (UAV). The CO<sub>2</sub> sensor selected was the Dynamet Premier CO<sub>2</sub> Infrared Sensor (Model MSHP/CO2/NC/5/V/P). This sensor contains all the necessary optics, electronics and firmware to provide a linearized, temperature compensated analog output. A Winsen Flammable Gas Sensor MQ-4 was selected for CH<sub>4</sub> sensing. This sensor is suitable for sensing CH<sub>4</sub> in air and can detect concentrations anywhere from 300 to 10000 ppm. Although this sensor is not as sensitive as, for example the LGR, it has a good sensitivity, fast response time and provides an analog output. An Arduino Pro Mini was used to convert the analog outputs of the two sensors and transmit the readings to a logging computer. The slung payload version of Zebgas was tethered to the end of a 10 m long cable, which required additional circuitry for an RS232 transceiver and a step-down regulator. A figure of the internals of the slung payload version of the Zebgas sensor can be found in the supplementary information (Supplementary information Fig. S1).

### 2.3.8. Unmanned Aerial Vehicle

A battery-powered octocopter was used to carry the Zebgas sensor as a slung payload and mounted with a Hovermap LiDAR (Kaul et al., 2016; Fig. 2). The octocopter has a flight endurance of 15 min while carrying the Zebgas and Hovermap payloads and was flown on 23 June. The slung payload consisted of the Zebgas sensor package and a 10 m power and data tether. The maximum swing on the slung payload when stopping or starting the UAV was  $\ll 20^\circ$ . A slung payload configuration was chosen over having the Zebgas sensor mounted to the UAV airframe as this allows the sensor to be suspended close to the ground while keeping the UAV at a safe height. It also ensures that the sensor is out of the down-wash from the UAV propellers, which could otherwise influence the gas concentration readings. More details on the configuration of the UAV and its sensors is given in Supplementary information Fig. S2. The octocopter uses a commercial off the shelf autopilot and is capable of manual (attitude stabilised), height hold and GPS waypoint-based flight. Hovermap is a 3D LiDAR mapping payload developed by the CSIRO Autonomous Systems Lab. By rotating a 2D LiDAR, a 3D spherical field of view is created, and the repeated views of the scene from each rotation allow sweep-match based Simultaneous Localisation and Mapping (SLAM), which can be then post-processed to produce a 3D point cloud of an area of interest and trajectory of the sensor origin.

### 2.3.9. Unmanned ground robot

The Husky robot (Clearpath Robotics) is a multipurpose 30 kg skid-steered mobile robot platform approximately 1 m  $\times$  0.67 m  $\times$  0.4 m in size and is suitable for indoor and outdoor environments. The standard platform, with no sensors, can carry up to a 20 kg payload in all-terrain conditions. Its maximum speed is 1 m/s. The robot has a typical 90 min endurance at 0.5 m/s. The CSIRO version of the Husky (Supplementary information Fig. S3) used in these experiments was fitted with an SBG-IG500n Inertial Measurement Unit (IMU) and a LMS-151 Sick LiDAR and the two gas sensing payloads (LGR and Zebgas). Surveys were taken on 22 and 23 June. It has an internal computer that is connected to all the payload components, as well as to an internal microcontroller that regulates all the low-level systems. The robot runs the Robot Operating System (Quigley et al., 2009). The IMU data are combined with wheel odometry using an Extended Kalman Filter (EKF) and fed into an on-line Simultaneous Localisation and Mapping (SLAM) system that uses the LiDAR scans to provide a 3D trajectory estimation. This system is accurate enough to navigate in semi-structured outdoor environments

autonomously. However, the experiments were done in an open field with no structure so the SLAM navigation system was not an option. Hence a GPS unit was added to the standard payload. Its readings were combined in the EKF to generate reliable trajectory estimations. A trajectory planner to execute predefined GPS-based waypoint trajectories autonomously was also designed and implemented for this project. The planner allows the Husky robot to execute survey, grid and spiral trajectories.

### 2.3.10. Mobile Picarro

A vehicle mounted Picarro G2201i cavity ring down spectrometer (CRDS) was driven in circuits around the release point from 15 May to 18 May by the University of Adelaide. Measurements of CH<sub>4</sub> concentration and  $\delta^{13}\text{C}$  were made every 3 s during the circuits, which were performed both during the day and at night. The sampling intake was at a height of 2 m, connected via a short hose attached to the CRDS. The circuits followed fences and roads on the property and also around the perimeter. The innermost circuit was between 50 m and 100 m from the release point, and the outermost at a distance of approximately 2 km. A GPS receiver was used to record the location of each measurement, taking into account the 40 s delay between a concentration change being presented to the intake, and it being recorded. A weather station was mounted on the roof of the vehicle. The system comprises a Rotronic temperature and humidity probe, a Vaisala barometric sensor and an RM Young Model 8100 3D sonic anemometer. Positional and time stamp data were collected using a Garmin GPS16X receiver; all time-stamped weather and positional data were logged to a Campbell Scientific CR1000 data logger.

### 2.3.11. Vertical scanning laser

In addition to the lateral scanning using an open path tuneable diode laser (TDL) described in Section 2.3.2, a system developed by the CSIRO was trialled that allowed both horizontal and vertical beam scanning through use of a UAV to carry the reflector target (Fig. 2). The goal was to measure the CH<sub>4</sub> concentration rapidly in a transect at any location across a plume. A Boreal GasFinder2 was mounted atop a pantilt unit and steered using an optical system to track the reflector while it was moving in three dimensions. Since the tracking approach was unorthodox, additional measurement modes were also performed in order to provide reference datasets. These were use of an Allsopp “Helikite” (a hybrid combination of kite and helium balloon) and a JLG 1500SJ Telescopic Boom Lift capable of 45.75 m maximum platform height. Photographs of the reflector platforms can be found in Supplementary information Figs. S4 and S5, respectively. In all three instances, an IMOS microcube reflector was attached and the platforms moved through various positions while the tracking system maintained pointing of the TDL sensing beam toward the reflector. The system was trialled from 22 to 23 June 2015.

### 2.3.12. Infrared cameras

A FLIR GF343 handheld infrared camera was tested for CO<sub>2</sub> detection by FLIR on 12 and 13 May. The CO<sub>2</sub> camera uses a cooled In-Sb focal plane array detector and detects over the 4.2–4.4  $\mu\text{m}$  spectral range. A FLIR GF320 handheld infrared camera was tested for CH<sub>4</sub> detection. The CH<sub>4</sub> camera uses a cooled In-Sb focal plane array detector and detects over the 3.2–3.4  $\mu\text{m}$  spectral range. Both cameras enable real-time optical imaging of gas leakage.

## 2.4. Quantification methods

Not all of the field instruments described above participated in the quantification exercise. For the blind quantification exercise, estimates of the emission rate were made using data collected by the following instruments: Eddy Covariance towers C, D and E; the two Picarro CRDS analysers; the Boreal GasFinder laser; the two open path FTIRs; and the LGR CRDS analyser. Data collected from the Husky robot equipped with

a LGR CRDS analyser were used in the quantification exercise once the release rate was known.

#### 2.4.1. Eddy covariance (EC)

**2.4.1.1. Eddy covariance data processing.** EddyPro software (V 6.0, LICOR) was used to process the collected data at 30 min time intervals. Applied quality control measures consisted of an angle of attack correction for the 3D sonic anemometer data (Nakai and Shimoyama 2012), time lag optimization, raw data statistical tests (Vickers and Mahrt 1997), de-spiking (Mauder et al., 2013), compensation for air density (Webb et al., 1980), and spectral corrections (Moncrieff et al., 1997, 2005). From here, the CH<sub>4</sub> flux data underwent a quality control screening system (0,1,2; according to Mauder and Foken 2004) where any 30 min time interval assigned a ‘2’ was removed. The remaining time points were filtered for CH<sub>4</sub> sensor signal strength (RSSI) values below 20, time points outside of the controlled release experiment (9:00–17:30), and a downwind direction  $> \pm 40^\circ$ .

**2.4.1.2. EC-forward Lagrangian stochastic (FLS) model.** After processing EC files in EddyPro and applying quality control filters as in Section 2.4.1.1, there were 44 and 155 thirty minute time points left from towers C and D respectively to predict an emission rate (g/min). A surface roughness of 0.005 m was calculated from neutral time points ( $0.02 \geq z/L \geq -0.02$ ) with a wind speed  $> 0.5$  m/s. Methane concentrations, temperature, pressure, and wind statistics from the 3D sonic-anemometer were used as direct inputs obtained from the EddyPro processed file. Using these inputs, a Forward Lagrangian Stochastic (FLS) model (Flesch et al., 1995) was performed using WindTrax (v2.0.8.8, Thunder Beach Scientific, 2013). The model was run using 50,000 trajectories for each 30 min time interval.

**2.4.1.3. EC-Lagrangian stochastic (LS) footprint model.** Data files from tower E were processed using EddyPro software following configuration and quality control protocols as described in 2.4.1 to calculate 30 min average fluxes. Average wind statistics, atmospheric stability, friction velocity and surface roughness length were used in conjunction with source and sensor coordinates to drive a Lagrangian stochastic (LS) footprint model (Coates et al., 2017). Briefly, the footprint procedure simulates the release of “particles” from the source with calculated trajectories based on modelled wind profiles. Trajectories which pass through the assigned sensor area are accumulated, and upon completion of the run, the theoretical relationship between the calculated flux at the tower and the source emission rate is obtained, expressed here as  $(F/Q)_{sim}$ . With the ratio calculated, the source emission rate ( $Q_{LS}$ ) can be inferred from Eq. (1),

$$Q_{LS} = F_{EC} \left( \frac{F}{Q} \right)_{sim} \quad (1)$$

where  $F_{EC}$  represents the calculated eddy covariance flux ( $\mu\text{mol CH}_4/\text{m}^2/\text{s}$ ). All model runs were based on a release of 500,000 particles and a sensor area described by a  $2 \times 2$  m horizontal plane.

#### 2.4.2. Atmospheric tomography using average line measurements

The atmospheric tomography method adopted here is based on the method given in Humphries et al. (2012) and uses the scanning Boreal laser data. A Bayesian inference framework was developed to estimate the release rate of a source where the concentration data are the line averaged concentrations from a scanning open path laser (Hirst, 2012), rather than concentrations from an array of point measurement sensors (Humphries et al., 2012; Jenkins et al., 2016). A Lagrangian stochastic (LS) model (Thomson, 1987) as implemented in WindTrax (v2.0.8.8, Thunder Beach Scientific, 2013) was used for forward modelling, i.e. to predict the concentrations given other parameters. We fitted a Gaussian plume model to the output of the Windtrax (a two dimensional array of concentrations) for a number of different stability conditions as

classified by the Monin-Obukov length. From this, plumes for a source of unit strength over a grid were generated and in this way a library of plume functions was built, which was an input to the Bayesian inference. The focus of the current work is the problem of quantification, although the Bayesian model allows for an easy reformulation to a problem of localisation. The Python code and accompanying user manual for estimating the emission rate using scanning laser data is available on GitHub (Bhatia et al., 2017).

Preliminary filtering was applied to the acquired Boreal laser dataset to discard rows with instrumentation errors or where the light level was deemed insufficient. Two datasets deemed to be of good quality were investigated for the blind release quantification experiment: 8–13 May and 11–18 May. The gas concentration data were averaged for each reflector over a 30 min period. Although this meant discarding a lot of information, this decision seems justified since the granularity of the weather information is no finer than 30 min. For each 30 min period, an average of the 5 lowest non-zero readings from each of the measurement paths was considered as the background concentration for that time interval. At very low wind speeds, the dispersion models usually break down. Hence measurements for the periods when wind speed was less than 1.5 m/s were not taken into consideration. Including low wind speed data in the analysis, decreased the estimate of the release rate and the posterior probability distribution was much less sharply peaked.

#### 2.4.3. Atmospheric tomography using point measurements

The atmospheric tomography technique applied here is based on the method given in Luhar et al. (2014) and it is applied using CH<sub>4</sub> concentration measurements acquired from the two Picarro instruments described in Section 2.3.1. Briefly, the technique uses an inverse model based on the Bayesian probabilistic approach, which updates the prior source knowledge through new concentration measurements. Given the difference in downwind and upwind concentration between the two Picarro instruments for a range of meteorological conditions (e.g. wind direction, wind speed, and atmospheric stability), and given the emission rate is constant with time, it is possible to use the data from all these periods together in one inverse modelling calculation to quantify the source. The source-receptor relationship required in the Bayesian model as the likelihood function is determined using a backward Lagrangian particle model. The Lagrangian model was driven by the following meteorological and turbulence quantities derived from the EC data: friction velocity ( $u^*$ ), the Monin-Obukhov length ( $L$ ), surface similarity relationships for the wind-speed profile, turbulent velocity variances and the turbulent kinetic energy dissipation rate. The aerodynamic roughness length ( $z_0$ ) for the area, which is required for the wind-speed profile, was estimated to be 0.01 m based on a matching of the observed wind speeds and those derived using the surface similarity relationship. Wind direction was taken from EC tower A. The spatial resolution of the backward Lagrangian stochastic model was  $5 \text{ m} \times 5 \text{ m} \times 1 \text{ m}$ . A more detailed description of the modelling approach is available in the Supplementary information M5.

Half-hourly data were examined from the period under consideration (09:00–17:00, 26 May–6 June 2015) and considered only those instances for which the mean wind direction from tower A was from outside the source sectors, which were defined as  $90^\circ$ – $156^\circ$  and  $295^\circ$ – $1^\circ$ . These source sectors correspond to  $\pm 3\sigma_y$  where  $\sigma_y$  is the lateral plume standard deviation estimated to be  $11^\circ$  for  $z_0 = 0.01$  m. Thus, the concentrations at both instruments during the above filtered periods represent the background concentration. The standard deviation ( $\sigma_b$ ) of the difference between the concentrations at the two instruments was then calculated using this data, which was 16 ppb for CH<sub>4</sub> and 1.7 ppm for CO<sub>2</sub>. We take  $3\sigma_b$  as the background uncertainty. Any source signal less than the background uncertainty will be difficult to detect. Therefore, for each species, we considered only those 30 min periods for which the observed magnitude of the concentration difference between the two Picarros is greater than the background uncertainty. Based on

that, the number of useful data points were 42 for CH<sub>4</sub> and only one for CO<sub>2</sub>. The model uncertainty was the error in the calculation of the source-receptor relationship, and consisted of two parts: statistical and structural, which are assumed to be 5% and 15%, respectively, of the computed value of the source-receptor coupling coefficient (Luhar et al., 2014).

#### 2.4.4. Backward Lagrangian stochastic model using open path FTIR spectrometers

Emission estimates of CH<sub>4</sub>, N<sub>2</sub>O and CO<sub>2</sub> were retrieved from data collected by the OP-FTIR systems using the backward Lagrangian stochastic (bLs) model as implemented in WindTrax (Flesch et al., 2004). Inputs to WindTrax included the mixing-ratio data as measured at each path downwind from the source, background mixing-ratio data and meteorological data including atmospheric pressure, temperature and wind statistical data from the 3D sonic anemometer. The paths downwind from the source were identified based on the compass bearing of the path, plus a 20° offset, and wind direction. Similarly background data was the average of data collected at all upwind measurement paths. As the bLs model is known to not perform well under non-favourable meteorological conditions (i.e. very stable atmospheric conditions, low wind speeds) (Wilson and Sawford, 1996) or uneven topography (non-level terrain, or presence of structure obstructing the windflow), data were removed based using the following filters: wind speed < 1.5 m/s, u\* < 0.15 m/s, and Zo > 5 cm. As P5 was located close to the source (closest point 4 m north of the source), data from P5 were not used in the WindTrax determination.

#### 2.4.5. Mobile measurement of tracer

In the tracer technique a stable gas unrelated to the source, such as C<sub>2</sub>H<sub>2</sub> or N<sub>2</sub>O, is released at a known rate,  $F_{Tracer}$ , from the same location as the CH<sub>4</sub> source. The tracer then mixes with the CH<sub>4</sub> and undergoes the same plume dispersion as the CH<sub>4</sub>. Simultaneous downwind measurements of the concentration enhancement (i.e. concentration above background) of both the tracer,  $C_{Tracer}$ , and CH<sub>4</sub>,  $C_{CH_4}$ , are made and the emission rate of CH<sub>4</sub>,  $F_{CH_4}$ , calculated according to Eq. (2):

$$F_{CH_4} = F_{Tracer} \times \frac{(C_{CH_4} - B_{CH_4})}{(C_{Tracer} - B_{Tracer})} \quad (2)$$

where  $B_{CH_4}$  and  $B_{Tracer}$  are the background concentrations of CH<sub>4</sub> and the tracer, respectively. A significant advantage of this technique over most other atmospheric approaches is that detailed meteorological data are not required to estimate the target gas emission rate.

During these experiments, the CH<sub>4</sub> and C<sub>2</sub>H<sub>2</sub> concentrations were measured at a rate of 1 Hz within the plume using the LGR CH<sub>4</sub>/C<sub>2</sub>H<sub>2</sub> analyser described in Section 2.3.6. Upwind measurements were also made periodically to determine the background CH<sub>4</sub> and C<sub>2</sub>H<sub>2</sub> concentrations.

In addition to the online analyses, we also collected a number of air samples for separate off-line analyses by FTIR. This allowed for the analyses and quantification of the CO<sub>2</sub> release rate (which was not available with the LGR instrument) as well as providing an independent check on the LGR CH<sub>4</sub> estimate. Air samples were collected into pre-evacuated 2.7 L Silonite™ canisters. Seven canister samples were taken, both upwind (background) and downwind (within the plume) of the emission source.

After collection, the samples were pressurised from ambient pressure to approximately 30 psi with nitrogen. A portion of the air sample was transferred into a 0.2 L cell containing a 2.4 m multi-reflection White cell. The air in the cell was analysed using a Nicolet 6700 FTIR analyser, with a resolution of 1 cm<sup>-1</sup>, utilising a liquid nitrogen cooled Mercury-Cadmium-Telluride detector operating between 700 and 4000 cm<sup>-1</sup>. Each sample was analysed at minimum in duplicate, with each analysis containing the co-addition of 256 scans.

The spectra were analysed for CH<sub>4</sub> and C<sub>2</sub>H<sub>2</sub> using classical least

squares fitting of the sample absorbance spectra relative to an instrument of the cell containing only nitrogen. Reference spectra for CH<sub>4</sub>, C<sub>2</sub>H<sub>2</sub>, N<sub>2</sub>O and CO<sub>2</sub> were calculated using the HITRAN database (Rothman et al., 2009). These were fit over specific spectral ranges using the MALT (Multiple Atmospheric Layer Transmission) software (Griffith, 1996) to generate mixing ratios for the targeted species.

Measurements were made over two consecutive days (26 and 27 May 2015) at distances up to 200 m from the release point. During this period, the CH<sub>4</sub> release rate was periodically varied between about half to three times the standard release rate of 5.8 g/min (Table 1), although the actual release rates were not revealed to the researchers. The CO<sub>2</sub> and C<sub>2</sub>H<sub>2</sub> rates remained constant during these periods at 100 g/min and 1.4 g/min, respectively (Table 1).

#### 2.4.6. Tracer gas (nitrous oxide) using open path FTIR spectrometers

The emission rate for CO<sub>2</sub> and CH<sub>4</sub> was retrieved from the OP-FTIR mixing ratio data using the N<sub>2</sub>O, released at a known rate, as a tracer gas in 2 ways. The CO<sub>2</sub> and CH<sub>4</sub> emissions estimated by the bLs model can be “corrected” by comparison with the bLs estimated N<sub>2</sub>O emission rate and the known release rate (Eq. (3)). While the bLs model does not perform well under non-favourable meteorological or topological conditions, any error introduced into the WindTrax estimated emission rate is independent of the gas released. With the 3 gases released within the same area, any error introduced to the emission estimate by the bLs model will be common to all gases. The comparison of the bLs target gas emission to the bLs tracer gas emission should increase precision and accuracy of the target emission estimates.

$$F_{gas} = \frac{WT(Gas)}{WT(N_2O)} \times F_{N_2O} \quad (3)$$

Where  $F_{gas}$  and  $F_{N_2O}$  are the unknown (gas) and known (N<sub>2</sub>O) emission rates, and  $WT(Gas)$  and  $WT(N_2O)$  are the WindTrax derived emission rates for the target and N<sub>2</sub>O tracer gas respectively.

More generally, as the release points of the gases are co-located, the emission rate of the target gas can be calculated from Eq. (4). This direct-tracer technique is a simpler and quicker method compared to the WindTrax-tracer (Eq. (3)) technique and, as the technique is not subjected to the same sources of error in WindTrax Model, the data quality filters can be reduced. In this work the filter originally imposed was a wind speed  $\ll 1.0 \text{ ms}^{-1}$ .

$$F_{gas} = \frac{\Delta[Gas]}{\Delta[N_2O]} \times F_{N_2O} \times \frac{MWT_{gas}}{MWT_{N_2O}} \quad (4)$$

Where  $F_{gas}$  and  $F_{N_2O}$  are as for Eq. (3),  $\Delta[Gas]$  and  $\Delta[N_2O]$  are the enhancement above background levels and  $MWT_{gas}$  and  $MWT_{N_2O}$  are the molecular weights, of the target gas and N<sub>2</sub>O tracer gas respectively.

#### 2.4.7. Gaussian plume fitting to mobile traverses

Attempts were made to quantify the emission rate of both methane and CO<sub>2</sub> using an atmospheric dispersion method in transects done with the Unmanned Ground Robot described in Section 2.3.9. In this technique, the CH<sub>4</sub> or CO<sub>2</sub> concentration profile in a plume originating from the source is measured at some distance downwind by performing traverses across the plume. This method, among others, was used by Day et al., 2014 to estimate CH<sub>4</sub> emissions from Australian coal seam gas well pads. By traversing across a plume downwind of the source, the emission flux,  $F$ , may be estimated by integrating the CH<sub>4</sub> (or CO<sub>2</sub>) concentration enhancement,  $C$ , of the plume in the horizontal ( $y$ ) and vertical ( $z$ ), directions and multiplying by the average wind velocity,  $u$ .

$$F = u \int_{-y}^y \int_0^z C(y, z) dy dz \quad (5)$$

Because concentration measurements are made only at ground level, the vertical dispersion must be estimated by reference to plume dispersion models such as the Pasquill-Gifford curves of  $\sigma_z$  (i.e. the

standard deviation of the distribution of CH<sub>4</sub> or CO<sub>2</sub> concentration in the vertical direction) as a function of down-wind distance under given atmospheric turbulence conditions (Hanna et al., 1982). The vertical concentration profile of CH<sub>4</sub> within the plume may be assumed to decrease from the ground level concentration with height according to a Gaussian distribution. Estimating the vertical extent of the plume introduces a significant source of uncertainty because the vertical concentration profile must be estimated from information on the spatial distribution of the source (i.e. an area or point source), downwind distance and prevailing atmospheric stability. Often these data are not well defined. In carefully designed experiments, ground based plume measurements can yield high levels of accuracy (e.g. Loh et al., 2009; Humphries et al., 2012). However, in less favourable conditions, such as the short term measurements made during this experiment, higher uncertainties are expected. A further source of uncertainty is that it is assumed that the ground level concentration measured during the traverse is the maximum concentration in the column, which may not be the case. Finally, because plumes tend to meander with short term wind variations, the dimensions of the plume and concentration profile can vary significantly over a short period of time. To minimise the uncertainty, it is necessary to make measurements over a number of traverses to provide an acceptable average. Day et al. (2014) conducted some controlled release experiments with methane to determine the uncertainty of this method. Average emission rates estimated from six traverses were generally within 30% of the actual release rate, although, individual traverses were found to vary by more than a factor of four in some cases. This technique was also used during the current experiment to estimate CH<sub>4</sub> and C<sub>2</sub>H<sub>2</sub> emission rates during May 2015. These measurements were made at downwind distances of between 15 and 90 m from the release point and the averages determined were within about 25% of the true emissions rate but again, there were substantial variations between individual traverses.

### 3. Results and discussion

#### 3.1. Detection

##### 3.1.1. Upwind-downwind point concentration measurements

Both the CO<sub>2</sub> and CH<sub>4</sub> concentrations were measured using the two “fixed” east and west Picarro analysers and the results are given in Figs. 3 and 4. The difference between these measurements is the perturbation above the background due to the CO<sub>2</sub> and CH<sub>4</sub> release. A strong diurnal signal is observed for CO<sub>2</sub> in Fig. 3, with high CO<sub>2</sub> levels present at night primarily as respired CO<sub>2</sub> is trapped in the stable atmospheric boundary layer. Lower CO<sub>2</sub> levels measured during the daytime are due to a combination of photosynthesis and greater atmospheric mixing. Good agreement for the concentration measurements is observed between both analysers for the majority of the experiment. Although the research field itself was bare of vegetation, the primary influence on the CO<sub>2</sub> concentration is from the surrounding farmland. For sites with more vegetation, higher night-time CO<sub>2</sub> concentrations may occur under stable atmospheric conditions and there could be increased CO<sub>2</sub> drawdown during the day (e.g. CO2CRC Otway site and Etheridge et al. (2011)). Fig. 3 highlights the challenge of detecting small parts per million perturbations above the high variable background signal even during the release periods and with a sensor located in an optimal downwind location. A greater difference between the two analysers is observed during a night release on 5–6 June 2015 and after 9 June, when the CO<sub>2</sub> release rate was increased from 100 to 300 g/min. A strong diurnal signal is not as evident in the CH<sub>4</sub> data and perturbations above the ~1.8 ppm background signal can be observed more clearly. The east Picarro was located approximately 100 m from the release source, downwind from the prevailing NW wind direction. Fig. 4 shows the difference between the concentrations measured by the two Picarras, and the excursions from zero reflect the times when the

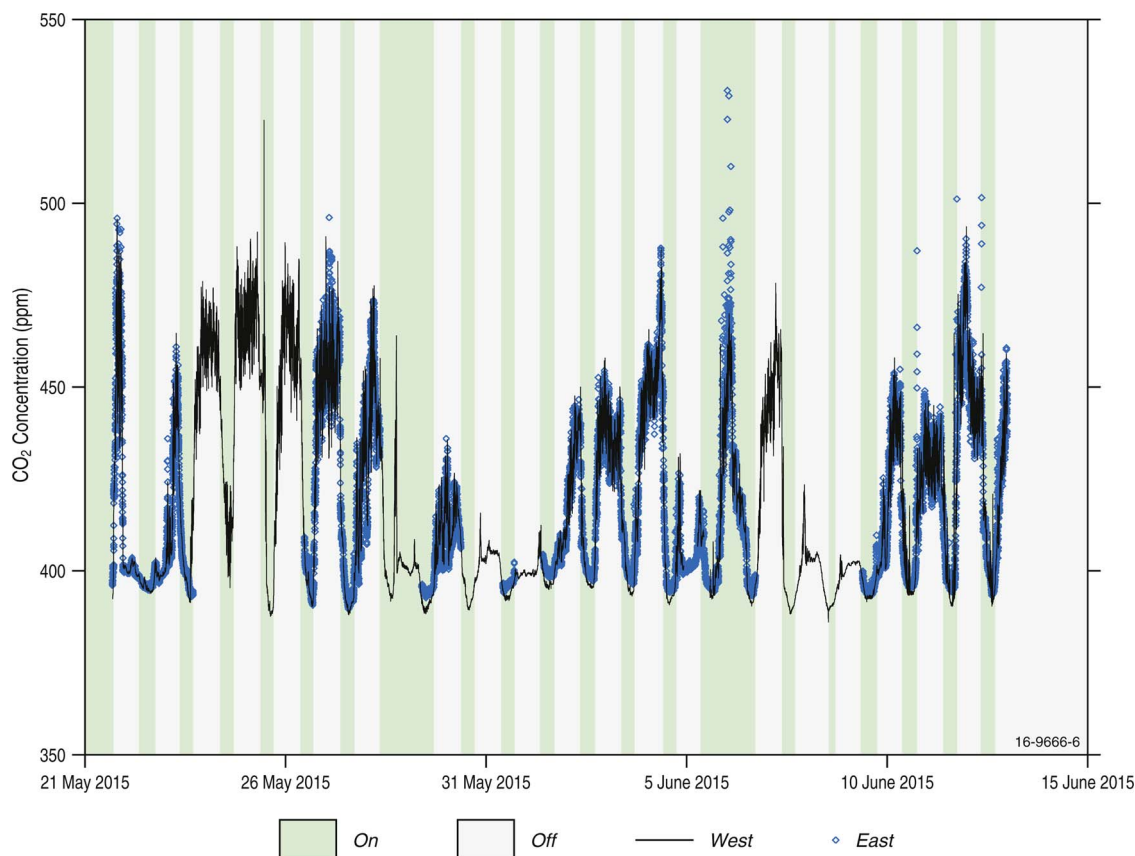


Fig. 3. CO<sub>2</sub> concentrations measurements using the east and west Picarro analysers.



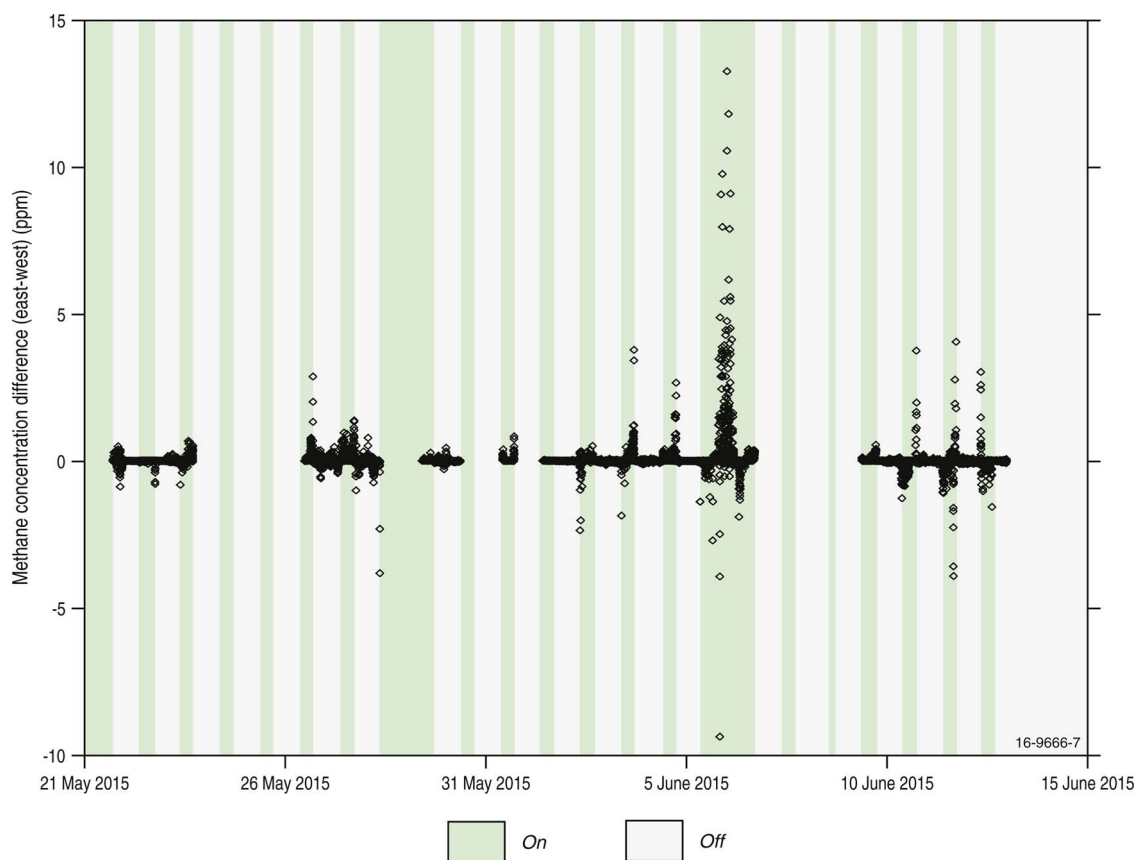


Fig. 4. Methane concentration difference plot between the east and west Picarro analysers (east minus west).

CH<sub>4</sub> plume was reaching one of the Picarro analysers but not the other. The maximum daytime downwind perturbation observed during the standard release rate (5.8 g/min), during well mixed conditions ( $u^* > 0.15$  m/s) was 1.59 ppm, but was mostly less than 0.27 ppm (95th percentile). The maximum CH<sub>4</sub> perturbation recorded was 13.27 ppm, at the east Picarro at 12:06 am on the 6/6/15 during an overnight release (Fig. 4). During this evening release, high CH<sub>4</sub> concentrations were recorded at both analysers (> 5 ppm), but not simultaneously. This indicates a significant accumulation of methane but also drifting of the plume between the two sensors under the stable night time conditions. A very high CO<sub>2</sub> perturbation was recorded at the same time (75.70 ppm). A maximum downwind daytime perturbation of 2.87 ppm was observed at the east Picarro during the 20 g/min release period.

### 3.1.2. Upwind-downwind flux measurements

When the wind aligned to have the plume from the emission source cross over a respective EC tower, a higher flux rate was recorded. Times of opposing wind directions produced background level flux rates. The EC towers proved to be useful in identifying the relative location of the emission source in addition to the flux rate (Fig. 5). Interpretation of the recorded flux ( $\mu\text{g}/\text{m}^2/\text{s}$ ) from the point source requires care, as the flux value recorded is highly dependent on the wind direction and the placement of the plume over the EC tower. For instance, tower A has a mean flux of 16.8  $\mu\text{g}/\text{m}^2/\text{s}$  compared to 6.4  $\mu\text{g}/\text{m}^2/\text{s}$  from tower D. This would be a product of the wind direction placing the CH<sub>4</sub> plume more favourably over tower A than D, and not the detection of a higher release rate (g/min).

### 3.1.3. Open path measurements

Both open path deployments (Boreal laser and FTIR) detected the CH<sub>4</sub> perturbation above background levels but there were substantial

differences in the precision and accuracy of the measurements (Fig. 6). The accuracy of the Boreal laser measurements was poor; the line-averaged background concentration CH<sub>4</sub> values measured  $\sim 1.6$  ppm compared to the true background value of  $\sim 1.8$  ppm measured using the Picarro analysers and FTIRs. Differences of  $\sim 0.4$  ppm CH<sub>4</sub> between the laser paths were typical for the Boreal laser measurements during periods of no CH<sub>4</sub> release (i.e. overnight in Fig. 6). Background measurements were between 2.6 and 3 times the reported limit of detection of 0.56 ppm m (Myers et al., 2000).

For the calibrated open path FTIR data, the average mixing-ratio from all paths between 8 and 13 May when gas was not being released was  $1780 \pm 6$  ppb for CH<sub>4</sub> (Fig. 6b) and  $326.8 \pm 0.8$  ppb for N<sub>2</sub>O. The average maximum increase in CH<sub>4</sub> above background was  $\sim 80$ – $220$  ppb,  $\sim 10$ – $20$  ppb for N<sub>2</sub>O. The CH<sub>4</sub> perturbations for the OP-FTIR (Fig. 6b) during the release periods are lower than for the Boreal laser measurements (i.e. approximately 100 m compared to 40–57 m, see Fig. 1). The Boreal laser and OP-FTIR can operate over distances up to 750 m and 400 m, respectively, but the optimum path length depends on the spatial size and magnitude of the leak. For CO<sub>2</sub> at the maximum flow rate (300 g/min; 9–12 June) the increase in above background levels was  $\sim 5$ – $10$  ppm.

### 3.1.4. Mobile detection techniques

**3.1.4.1. Vehicle mounted Picarro.** The capability of the Picarro G2210i to detect the <sup>13</sup>CH<sub>4</sub> isotopologue is a valuable tool to distinguish different emissions of methane CH<sub>4</sub> from different sources. The farm had sheep nearby the release site from time to time, usually NE or NW of the release point. The accuracy of the  $\delta^{13}\text{C}_{\text{CH}_4}$  measurements with this particular CRDS is about 5‰, but it is very reproducible (ca 1‰ with sufficient averaging) and gives reliable relative measurements. Fig. 7 shows measurements obtained at 09:00 on 18 May, driving each of the

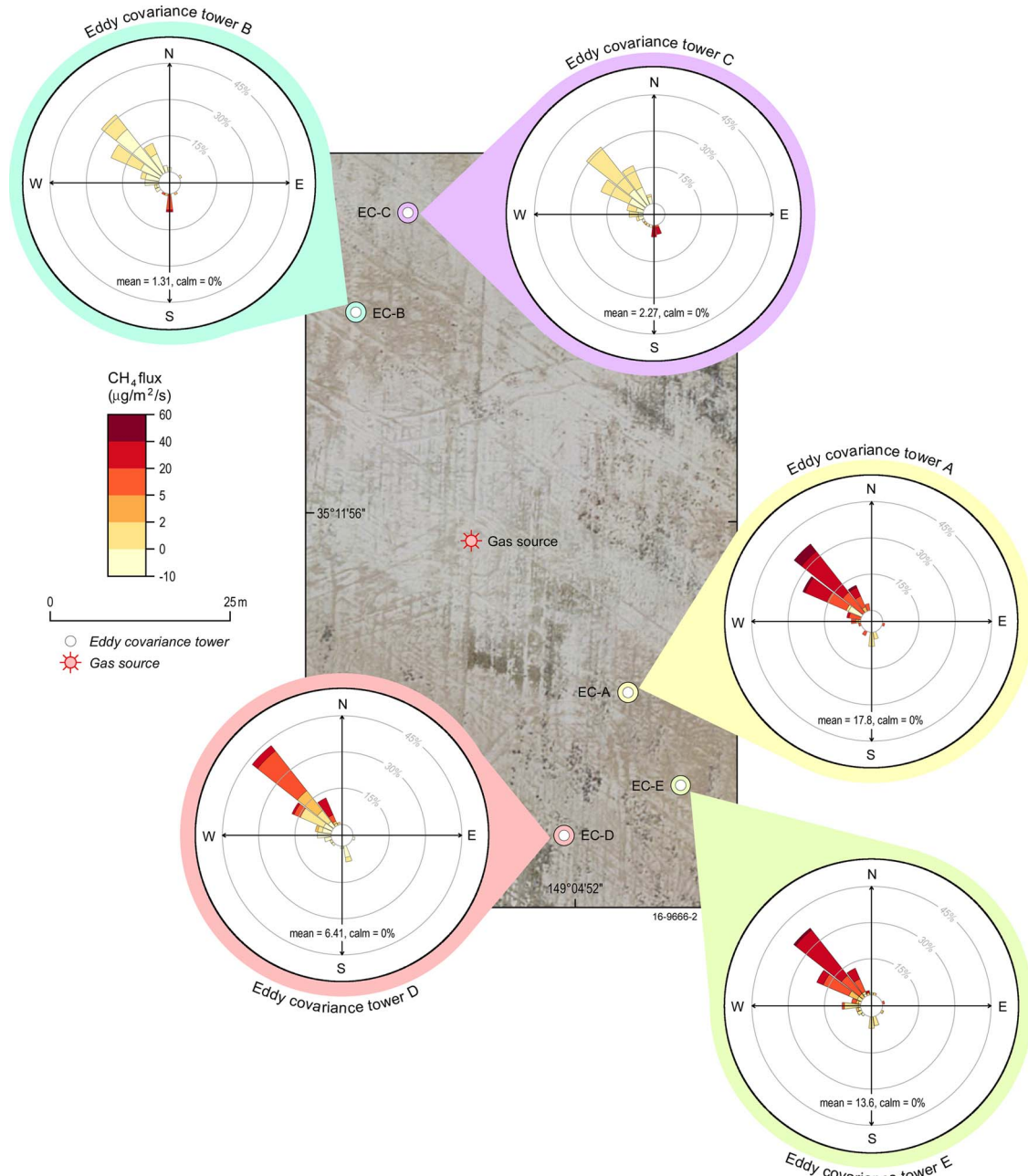


Fig. 5. Flux wind roses for the 5 EC towers showing the predominant upwind and downwind wind directions. The values presented in each windrose is the mean 30 min  $\text{CH}_4$  flux (in  $\mu\text{g}/\text{m}^2/\text{s}$ ) from all measurements that passed the EddyPro filtering process.

circuits (except the outermost) two times. While driving the inner two circuits at the start of the measurement, the wind speed was weak ( $\sim 1$  m/s) and from the SE. When taking measurements from the outermost circuit the wind speed strengthened and the wind direction shifted to the NE. The plume from the controlled release is clearly visible close to the release point, and a substantial peak is also seen where a flock of sheep was encountered. The colour scale indicates the  $\delta^{13}\text{C}$  measurement, showing that the  $\text{CH}_4$  from the sheep is clearly distinguishable from that of the release.

**3.1.4.2. Unmanned ground robot.** Methane concentration data from the Los Gatos Research  $\text{CH}_4/\text{C}_2\text{H}_2/\text{H}_2\text{O}$  analyser collected during the Husky UGR runs were examined to determine their suitability for estimating emissions flux. In one of the runs, the robot collected data while executing a squared spiral trajectory from the release point. The process took 35 min at a constant speed of 0.5 m/s. Figs. 8 and 9 show the GPS-

located  $\text{CH}_4$  concentration data collected by the LGR and Zebgas (Winsen) sensors. LGR  $\text{CH}_4$  concentration data are shown in ppm, while the Zebgas concentrations are shown in mV.

The Winsen  $\text{CH}_4$  sensor data correlated well with the data collected using the LGR during the surveys near the release source. After correcting for a lag of approximately 20 s for the LGR using 1D correlation, the Winsen sensor demonstrated a similar rise time to the LGR but had a longer fall time (Supplementary information Fig. S7). Based on comparisons with the LGR, the Winsen sensor appears to be able to detect  $\text{CH}_4$  perturbations of less than 5 ppm. This detection limit is much less than the reported sensitivity of 300–10,000 ppm.

**3.1.4.3. Unmanned Aerial Vehicle.** The UAV data were collected by flying a pre-programmed flight path in the form of parallel transects. The transects were aligned with the paddock fences and not according to the wind direction. The wind direction was considered when

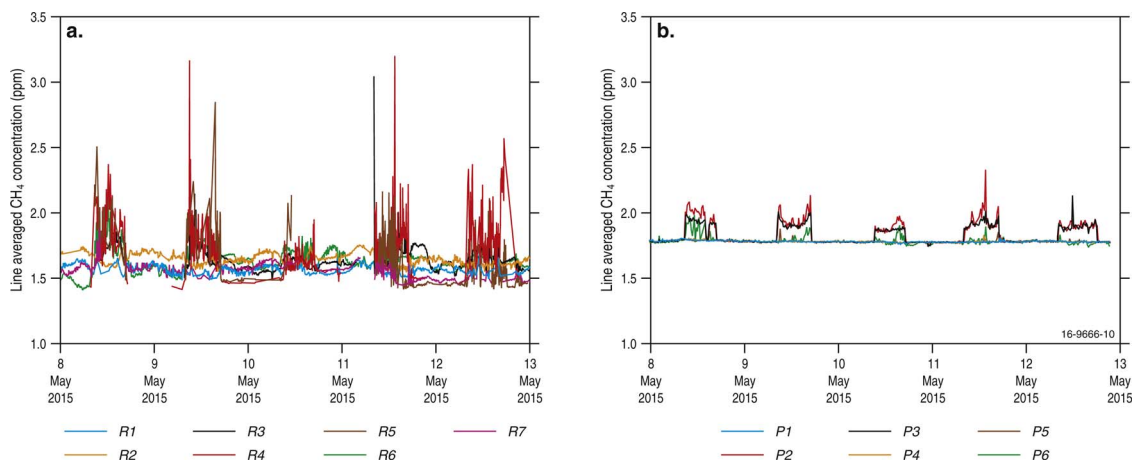


Fig. 6. Comparison of 30 min averaged open path CH<sub>4</sub> measurements using the (a) Boreal laser and (b) OP-FTIR spectrometers for 8–12 May. R1–R7 in (a) refers to the paths from the scanning laser to each of the retro-reflectors in the field and P1–P6 in (b) refers to the OP-FTIR paths (see Fig. 1 insert).

determining start and end of the transects to ensure at least one transect was upwind of the release point. The flight altitude was set to 11 m to ensure the slung payload remained approximately 1 m above the ground (10 m tether length). The paddock is essentially level so there was no need to adjust the height during flight to match the terrain.

Although the Hovermap payload was carried and lidar data were logged, we did not expect the SLAM navigation system to work since the terrain was open with very few 3D features. For this reason we also logged GPS data during the flight. Surprisingly, one of the UAV flights produced valid SLAM results so we were able to overlay the gas data on the SLAM-generated trajectory (see Supplementary information Fig. S8). For the other flights the GPS trajectory was used. The GPS and SLAM measurements produce the trajectory of the UAV, not that of the gas sensors at the end of the tether 10 m below. Since a pendulum motion was induced in the slung payload it was not always directly below the UAV. It is therefore only possible to estimate the true position of the gas sensors from the GPS and SLAM trajectories. The figures in this section are therefore estimates of the gas concentrations at the plotted locations.

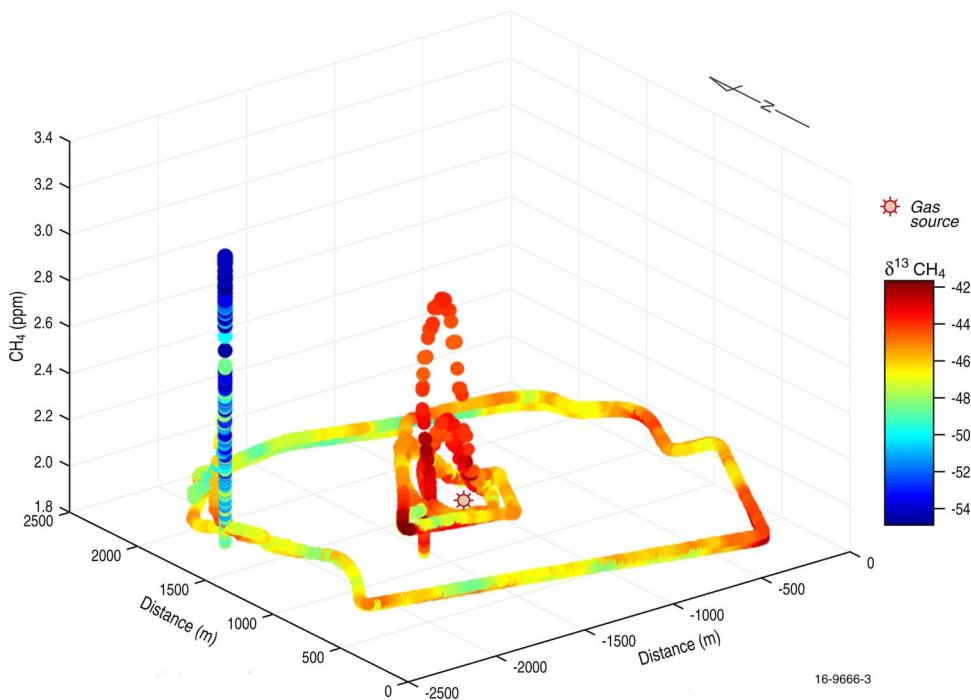


Fig. 7. Methane concentration (vertical axis) as a function of position, measured on 18 May by the mobile Picarro. The release point is indicated by the red dot, and the colour indicates the measured isotope ratio  $\delta^{13}\text{C}$ . The CH<sub>4</sub> source had an isotope signal of  $\delta^{13}\text{C} -38.9 \pm 0.29\%$ . The  $\delta^{13}\text{C}$  depleted blue response in the figure corresponds with the location of a flock of sheep approximately 1 km from the release chamber. (For interpretation of the references to colour in this figure legend, the reader is referred to the web version of this article.)

Figs. 10 and 11 show the results for one of the four flights conducted. The flight test was conducted by flying a pre-programmed set of GPS waypoints which formed 9 transects. The flight speed was set to 1 m/s and the average wind speed was 2.3 m/s. Fig. 11a and b depict the Zebgas Winsen CH<sub>4</sub> readings in mV and overlaid on the GPS trajectory respectively. Fig. 12a and b depict the Zebgas Dyanment CO<sub>2</sub> readings in ppm and overlaid on the GPS trajectory. Both figures illustrate that the Winsen and Dyanment sensors within the Zebgas were unable to adequately resolve the CH<sub>4</sub> and CO<sub>2</sub> plumes, using the UAV platform at a flight speed of 1 m/s and at 1 m sensor elevation.

### 3.1.5. Hyperspectral and infra-red detection

From the data acquired by the Bruker HI90 at 100 m from the controlled release, we were able to identify the gas released as CH<sub>4</sub>, capture the spatial distribution and provide an indication of relative abundances based on spectral matching with a reference library of methane and other gases (Harig et al., 2003). A video of the methane release (Fig. 12) illustrates the challenges of modelling the CH<sub>4</sub> plume. The plume is observed to periodically snap off, despite the constant

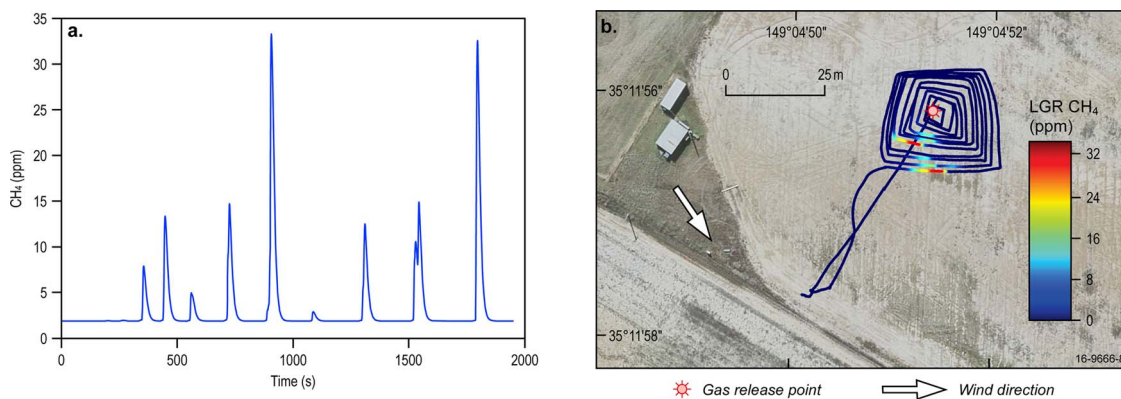


Fig. 8. LGR CH<sub>4</sub> measurements over time and on their GPS trajectory. The rover moved in a clockwise direction and a significant measurement delay in the elevated CH<sub>4</sub> response can be seen for the LGR compared to the Winsen sensor (Fig. 9b).

release rate, and wander as the wind direction changes. The majority of rate estimate techniques in this study rely on coupling concentration measurements with a plume model (e.g. WindTrax); hence having a good model of the plume is essential for an accurate rate estimate.

The instrument was relocated to the top of a small hill some 1.5 km from the release point. Although, methane absorption features were detected in the spectra collected (Supplementary information Figs. S9 and S10) it was constrained by dilution due to the wind and the measurement distance. Therefore, it was difficult to identify the release area as an anomaly separate from ambient methane at such a large distance. However, measurements performed using the instrument at an abandoned borehole in Chinchilla, Australia, showed that detection of small emissions of methane was possible at distances up to 500 m (Etheridge et al., 2016).

It was just possible to observe CH<sub>4</sub> using the handheld FLIR GF343 CO<sub>2</sub> optical camera at 20 g/min close to the release chamber (Supplementary information Fig. S11); however, this rate appears to be close to the limit of detection for this instrument for this type of emission configuration. Greater success was observed with the FLIR CO<sub>2</sub> camera at 100 g/min where the CO<sub>2</sub> emission could be clearly observed [Supplementary information Fig. S12].

3.1.6. Vertical scanning laser

Data from this system consisted of CH<sub>4</sub> line-integral concentration measurements co-recorded with (1) pan-tilt pointing values, (2) geometrically and laser-ranging determined distances to target, and (3) weather measurements (wind speed, direction, air temperature and pressure). These enabled reconstruction of the instantaneous reflector target 3D positions and associated line-integral concentrations. An additional GPS surveying procedure enabled geodetic registration of the complete dataset to additionally incorporate measured wind speed and

direction. The intention was to use measurements from the line-average concentrations as a function of scan height above the source to create vertical profiles of the plume. Unfortunately it was discovered that the second Boreal GasFinder2 TDL instrument used had a significant calibration fault and required to be returned to the manufacturer for repair. Due to timing constraints this fault was not clearly identified until after the Ginninderra experiment and the data could not be confidently post-corrected for the fault. Nonetheless, the principle goal of validating this novel approach to emissions monitoring and plume circumscription was sufficiently demonstrated and further work is underway to optimise the technique. The tracking system worked well with both the moving UAV and telescopic boom lift (refer to Supplementary information R5) but did not work with the Helikite. A similar approach has been recently demonstrated by Cossel et al. (2017) using high-precision dual-comb spectroscopy to a retroreflector mounted on a flying multicopter.

3.2. Quantification

3.2.1. Summary and ensemble estimate

A workshop was held at Macquarie University, Sydney, on 1 December 2015 where the participating teams presented their blind estimates of the release rate. A summary of the results presented at the workshop is given in Table 3. The majority of the average emission methane estimates were within 20% of the release rate for the blind estimates and within 10% after the known rate was revealed. However, the confidence intervals supplied with each blind estimate submission did not contain the true mean. The study is a useful reminder that one should not conflate the uncertainty of an individual emission estimate with a range that contains the true mean.

Taking an ensemble approach to the emission rate estimates (Wilks, 1995) provided an accurate estimate the actual emission rate and

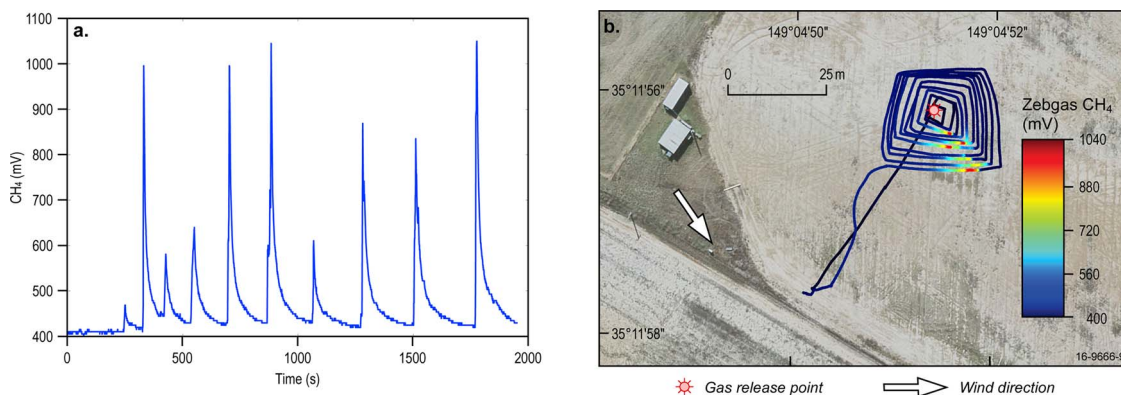


Fig. 9. Zebgas (Winsen) CH<sub>4</sub> measurements over time and on their GPS trajectory. The rover moved in a clockwise direction.

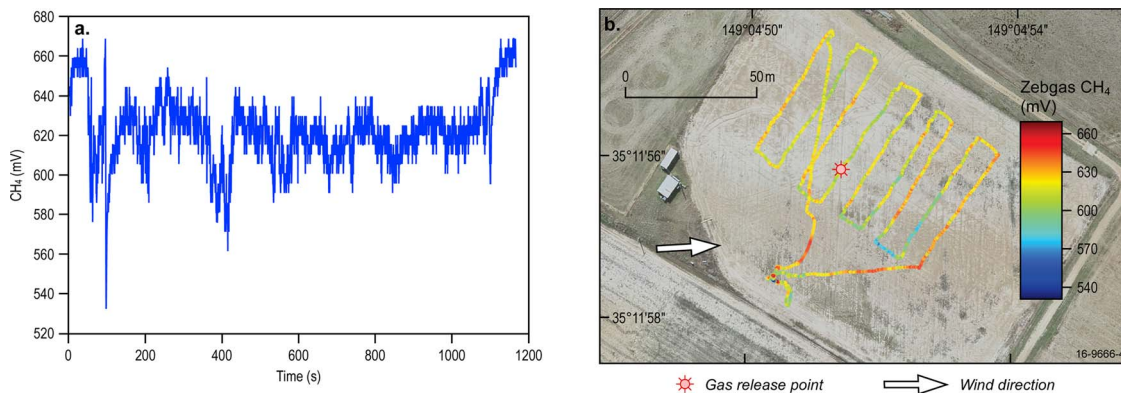


Fig. 10. Zebgas Winsen CH<sub>4</sub> ADC readings in mV (a) and overlaid on the UAV GPS trajectory (b).

provided a more useful measure of the uncertainty (i.e. it included the actual release rate). Ensemble mean or median approaches are routinely used in numerical weather or climate predictions (Toth et al., 2003) and have been observed to frequently outperform individual models (Lambert and Boer 2001). Annan and Hargreaves (2011) explained the performance of the multimodel mean in the context of the statistically indistinguishable paradigm and that the truth and models are drawn from the same distribution.

The ensemble median of the methane estimates was more representative of the true emission than the ensemble mean due to the non-normal distribution of the emission estimates (Table 3), particularly for the blind estimates. The ensemble mean for the blind estimate was 11.9 g/min but the median estimate was 6.7 g/min (within 16% of the true release rate). The uncertainty of the blind estimates was broad, ranging from 4.75 to 46.9 g/min. The range for the methane estimates narrowed markedly once the rate was known (4.75–6.31 g/min) and the ensemble mean for the blind estimate was 5.77 g/min (within 1% of the actual release rate) and the median estimate was 5.90 g/min (within 2% of the actual release rate). The improvement in the estimates once the release rate was known was generally achieved by applying more stringent filters to the concentration data (e.g. wind direction, wind speed and atmospheric stability) and is discussed further in the following sections. Individual estimates lay above or below the actual release rate in all cases suggesting there was no model bias.

The closest individual CH<sub>4</sub> estimate during the standard 5.8 g/min blind release period was 5.9% lower than the actual release rate and was achieved using the acetylene tracer ratio technique (Table 3). During the 5 day period immediately after the standard release (Table 3), where the CH<sub>4</sub> release rate was lowered to 5 g/min and CO<sub>2</sub> release rate increased to 300 g/min, the FTIR–N<sub>2</sub>O tracer gas method continued to operate and provided a very close blind estimate for both CO<sub>2</sub> and CH<sub>4</sub>, i.e. within 0.5% for CH<sub>4</sub> and 7% for CO<sub>2</sub>. The results,

assumptions and limitations for each of the individual quantification methods used in the ensemble are described in more detail in the following sections.

The cost of the instrumentation was not a consideration in this quantification inter-comparison yet is important for an operator or service provider. It is beyond the scope of this paper to undertake a full economic and practicality analysis, but an indication of the relative costs of the instrumentation deployed during this study is provided in Table 3. Superficially, the most expensive methods were those that used two instruments with high capital costs (the dual OP-FTIR and dual Picarro analysers) and the least expensive was the canister sampling coupled with the C<sub>2</sub>H<sub>2</sub> tracer. But the practicalities of each method also need to be considered: whether the instrumentation can be solar powered versus requiring access to electricity from the grid; the degree of automation possible; reliability; calibration stability; remote access; and the degree of manual handling. Canister sampling has the advantage of being quick and comparatively less expensive, but it only takes a snapshot in time and requires accurate metering of a tracer in the field which may not be possible. The continuous methods deployed in the study have the advantage of being able to average emissions over a period of days to weeks, which may produce a more representative estimate especially if there is variability in the emission rate. Supplementing continuous measurements with canister and tracer sampling appears to be a good strategy for accurate quantification of emissions.

### 3.2.2. Eddy covariance

Traditionally, eddy covariance (EC) micrometeorological methods are used to measure air-surface exchange of a scalar quantity, such as CH<sub>4</sub> concentration, when all theoretical and physical constraints of the methodology are met. The CH<sub>4</sub> flux measured is therefore representative of a footprint defined during a stationary meteorological period by the prevailing atmospheric conditions. It was not expected

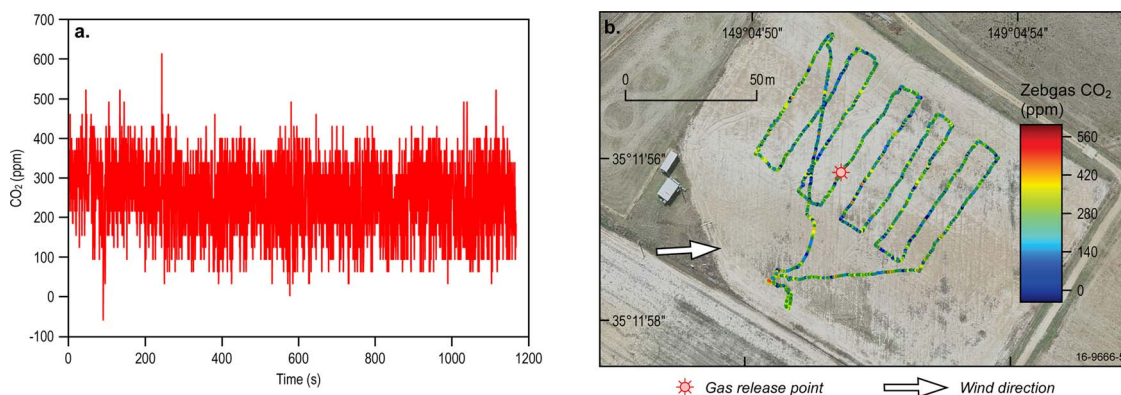


Fig. 11. Zebgas Dynamet CO<sub>2</sub> readings in ppm (a) and overlaid on the UAV GPS trajectory (b).

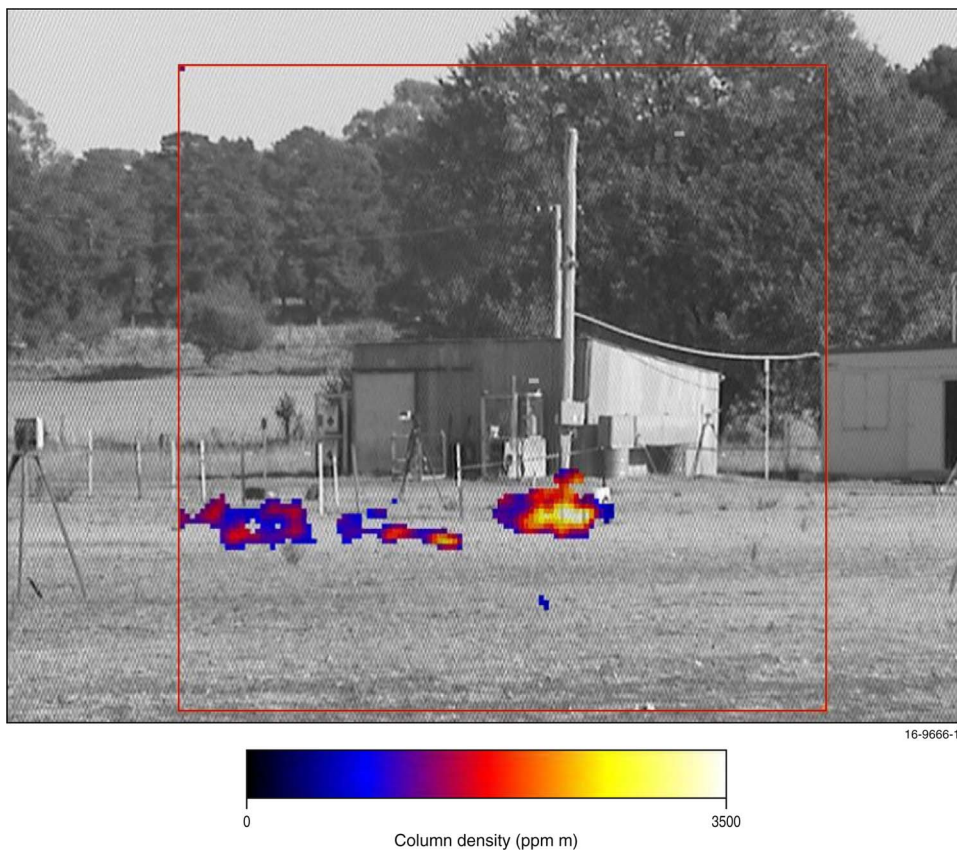


Fig. 12. Column densities of methane derived from the spectral measurement using the Bruker HI90 at 20 g/min release rate at a distance of 100 m. The red box illustrates the region of methane recordings. (For interpretation of the references to colour in this figure legend, the reader is referred to the web version of this article.)

**Table 3**  
Summary of blind and known estimates of the CO<sub>2</sub> and CH<sub>4</sub> emission rates with 95% confidence intervals.

Organisation	Technique <sup>a</sup>	Relative instrumentation cost <sup>b</sup>	Days used for “Blind” rate calculation	“Blind” rate estimate CH <sub>4</sub> g/min	“Blind” rate estimate CO <sub>2</sub> g/min	Days used for known rate calculation	Known rate estimate CH <sub>4</sub> g/min	Known rate estimate CO <sub>2</sub> g/min
UoW	N <sub>2</sub> O tracer	+++	23	6.8 ± 0.63	186 ± 46	9	6.02 ± 0.32	–
UoW	FTIR – bLS	+++	21	6.6 ± 0.5	192 ± 57	13	6.04 ± 0.29	–
UoW	WT	+++	–	–	–	9	6.31 ± 0.37	–
UoM	EC – LS footprint model	++	27	7.01 ± 0.56	83.9 ± 12.8	22	6.26 ± 0.37	–
MQ/UoA	EC – FLS	++	18	46.9 ± 26.9	–	18	5.6 ± 1.9	–
CSIRO	Mobile tracer – C <sub>2</sub> H <sub>2</sub>	++	≪0.05	5.46	–	≪0.05	5.9 ± 0.05	–
CSIRO	Mobile tracer – canister	+ <sup>c</sup>	10 <sup>–3</sup>	5.1	115 ± 23	10 <sup>–3</sup>	4.75 ± 0.6	106 ± 24
GA/WS	AT – line	++	6	4.86 ± 0.66	–	6	5.83 ± 0.6	–
CSIRO	AT – point	+++	11	12.3 ± 0.66	3640 ± 1750	11	5.22 ± 2.2	–
<b>Ensemble mean</b>				<b>11.9</b>	<b>843</b>		<b>5.77</b>	
<b>Ensemble median</b>				<b>6.70</b>	<b>186</b>		<b>5.90</b>	
Actual release rate				5.80 ± 0.06	100 ± 1.0		5.80 ± 0.06	100 ± 1.0
Other release rates								
UoW	N <sub>2</sub> O tracer	+++	4	4.97 ± 0.14 <sup>d</sup>	279 ± 101 <sup>d</sup>	4	4.97 ± 0.14 <sup>d</sup>	
CSIRO	Mobile traverse	++				≪0.05	10.2 ± 7.4 <sup>e</sup>	459 ± 153 <sup>e</sup>

<sup>a</sup> Technique abbreviations: N<sub>2</sub>O tracer (open path FTIR with N<sub>2</sub>O direct tracer ratio technique); FTIR-bLS (open path FTIR with backwards Lagrangian stochastic modelling); WT (open path FTIR with N<sub>2</sub>O coupled Windtrax modelling); EC – LS footprint model (eddy covariance with Lagrangian stochastic footprint modelling); EC – FLS (eddy covariance with forward Lagrangian stochastic modelling); Mobile tracer – C<sub>2</sub>H<sub>2</sub> (mobile Los Gatos Research analyser with C<sub>2</sub>H<sub>2</sub> tracer); Mobile tracer – canister (canister measurements with C<sub>2</sub>H<sub>2</sub> tracer); AT – line (atmospheric tomography using the Borealis scanning laser); AT – point (atmospheric tomography using the two fixed Picarro instruments); Mobile traverse (mobile robot traverses with Gaussian plume modelling).

<sup>b</sup> + < \$10,000; ++ \$10,000 < + < \$200,000; +++ > \$200,000. In Australian dollars.

<sup>c</sup> Cost assumes analysis at commercial laboratory but includes cost of tracer ancillaries including mass flow controller, acetylene and canister.

<sup>d</sup> For 5.0 g/min CH<sub>4</sub> and 300 g/min CO<sub>2</sub> release rates (8–12 June).

<sup>e</sup> For 20 g/min CH<sub>4</sub> release and 300 g/min CO<sub>2</sub> release.

(and was verified) that the dry bare soil substrate would be producing a background CH<sub>4</sub> flux however local sources could influence measurements due to local advective effects. In the absence of any local effects, the plume from the experiment's point emission source would be seen by those towers where the wind direction directly aligns with the towers and the source. However, due to the variable nature of the wind direction and turbulent wind field, the plume dispersion and plume centre line is likely to vary considerably. It is therefore unknown where exactly the source plume was and how much of the plume was seen by any point average measurement of the trace gas at an EC tower. In this study the EC groups (University of Melbourne and Macquarie University/University of Adelaide) coupled EC measurements with atmospheric modelling approaches to estimate an emission rate.

**3.2.2.1. EC forward Lagrangian stochastic (FLS) approach.** The Ginninderra measurement scenario presented a point source emission. Through evaluation of the EC flux in wind sectors not aligned with the point source, the bare soil at the Ginninderra site was determined not be a source or sink of CH<sub>4</sub>, and hence not influencing the towers flux footprint. Examining the fluxes in aligned wind sectors demonstrated that the CH<sub>4</sub> sensor saw the plume from the point source, but, as would be predicted, the EC flux measurement was not able to determine the point source emission rate. To obtain the rate we used the CH<sub>4</sub> concentration measurement from the tower coupled with a forward Lagrangian stochastic model to predict the point source emission rate.

A blind release estimate of 46.9 g/min (Tables 3 and 4) was made, which was an overestimate by a factor of >7 of the actual emission rate (5.8 g/min). Using a point-sensor to estimate a point-source emission rate relies heavily on the accuracy of the atmospheric data. While data from a 3D sonic anemometer is sufficient, its initial setup within WindTrax can be complicated, and as seen here may require optimisation. The logging program for Towers C and D required the anemometers' 'U' spar marker, for north, to face exactly north to produce an accurate wind direction, but it was mounted slightly (~10°) to the NW. The slight offset (offset angle) directly impacted the computed wind direction in WindTrax. Therefore, the known wind direction produced from the Eddy Pro® software was added to the WindTrax input file and monitored against the Windtrax computed wind direction. This procedure allowed for the offset angle to be precisely adjusted and input into the Windtrax 3D anemometer setup. After 3D anemometer optimization, an estimated emission rate of 4.6 g/min was produced from the downwind tower (D). This prediction underestimated the actual emission rate by 21%. An optimized emission rate of 5.6 g/min (Table 4) was reached through applying a more stringent filter for wind direction (±15°) and for very unstable and very stable atmospheric conditions (−0.2 < z/L < 0.2).

The upwind tower (C) mostly missed the point source's emitted plume, providing only eight usable 30 min time points to predict an emission rate (Table 4), and none once the more stringent filters for wind direction and atmospheric stability were applied. Here, tower D, placed in the predominant downwind direction, successfully predicted an emission rate from a point source. However, two or more towers can be used to optimize data capture and enhance confidence. These advantages need to be tested in a scenario where multiple sources/sinks are present within a towers footprint.

**3.2.2.2. EC – Lagrangian stochastic (LS) footprint approach.** Application of the LS footprint model allowed for a direct estimate of emission rate based on the EC generated flux at tower E. The first “blind” estimate of source emission was obtained by applying a conservative set of filters to the dataset to exclude periods where; 1) wind direction exceeded ±45° from the source, 2) the friction velocity was less than 0.08 m/s, 3) atmospheric stability was very stable (z/L ≥ 0.95) or very unstable (z/L ≤ −0.95). In addition any periods where battery voltage was less than 11.2 V or Li-7700 signal strength was less than 20 were removed.

With the release rate known, it was found that a reduction in the

range of acceptable wind directions was required to prevent underestimation of the emission rate for measurements based on edge of plume wind directions. Atmospheric stability was also found to impact the accuracy of emission estimates with unstable periods yielding estimates 50% greater than those from neutral or stable periods. More stringent filters for wind direction and atmospheric stability led to a more accurate mean estimate of the emission rate (Table 5). An additional filter was also added to exclude periods when the random error component of the EC flux exceeded 25%. Application of revised filters reduced the overestimate of emission rate from 21% to 8% (Table 5).

### 3.2.3. Atmospheric tomography integrated line technique (ATL)

At the methane workshop, two estimates for the average methane release rate were provided for the ATL technique: 4.86 ± 0.66 g/min (11–18 May) and 6.6 ± 1.0 g/min (8–13 May). The 4.86 g/min value was lodged for the final blind estimate but the 6.6 g/min estimate for the 8–13 May time period was closer (14%) to the actual release value of 5.8 g/min. A comparison between the datasets for the two estimates is instructive. The 8–13 May dataset was more continuous but suffered from smaller 30 min averaged methane perturbations compared to the 11–18 May dataset. Also, there are only 2 values (both path R5) significantly above the background noise on May 10 (Fig. 13a). If the day to day estimates for the release rate are determined for the 8–13 May dataset, it can be seen than the majority of the average estimates are close to the actual release rate of 5.8 g/min (Fig. 13b). Only 2 values along the same path (R5) were insufficient to resolve the estimate on May 10 and led to a substantial underestimate of the release rate (2.1 g/min). An apparent overestimate of the release rate can be observed on May 13, with the average value suggesting 18.9 g/min. On closer inspection of the data collected that day, there was a brief 20 min period where the release rate was increased from 5.8 to 20 g/min in order to test the sensitivity of the FLIR handheld camera. The 18.9 g/min estimate is remarkably close to the high release rate (within 5.5% of the actual release rate) and suggests that the ATL technique is strongly weighted towards determining maximum estimates given the available data. This may be a function of the constant release rate assumption in the Bayesian inversion. If the 20 min high CH<sub>4</sub> release rate period is removed from the 8–13 May dataset, the revised methane rate estimate over the 8–13 May period increases to 5.83 g/min and is close to the actual release rate (within 1.0%).

### 3.2.4. Atmospheric tomography point measurement technique

As noted earlier, the term atmospheric tomography is used interchangeably with inverse atmospheric modelling for source estimation. To illustrate how prior knowledge of the source location influences the source estimates, we performed two Bayesian simulations for CH<sub>4</sub> source estimation. In the first, a Gaussian prior was specified for the

**Table 4**  
Point-source-to-point-sensor CH<sub>4</sub> emission rate (g/min) outputs using a forward Lagrangian stochastic (FLS) in Windtrax for a) the blind estimate where both towers were combined, b) 2nd attempt after optimizing Windtrax parameters using the tower D time points, c) 2nd attempt when filtering for atmospheric stability using the tower D time points, and d) 2nd attempt after optimizing Windtrax parameters using tower C time points.

	Blind release Towers C + D	Known release towers D	Known release <sup>a</sup> tower D	Known release tower C
Average (g/min)	46.9 <sup>a</sup>	4.6 <sup>b</sup>	5.6 <sup>c</sup>	7.9 <sup>d</sup>
Median	44.5	4.5	5.3	7.7
Std. dev.	26.9	2.2	1.9	5.2
N (30 min time points)	35	75	25	8

<sup>a</sup> Filtered for wind direction (±15°) and stability (−0.2 < z/L < 0.2).

**Table 5**

Cumulative effect of revised filters on the mean and median emission rate estimates (and 95% confidence interval) for the standard rate of 5.8 g/min. N represent the number of 30 min periods. First row is filtered to include only data where friction velocity ( $u^*$ ) is  $>0.08$  m/s, flux quality flag (after) is less than two and stability falls within the range of  $-0.95 < z/L < 0.95$ . Final row represents the final estimate.

Filter applied	Known rate estimate of CH <sub>4</sub> (g/min)		
	n	mean	median
Revised wind direction filter $\pm 30^\circ$	194	7.17 $\pm$ 0.50	6.62
Revised stability filter $-0.09 > z/L > 0.5$	149	6.36 $\pm$ 0.41	5.99
Additional filter, EC random error $< 25\%$	135	6.26 $\pm$ 0.37	5.90

source location ( $x_s, y_s, z_s$ ) centred at the real source with standard deviations of  $\sigma_{x_s} = \sigma_{y_s} = \Delta x = 5$  m and  $\sigma_{z_s} = 0.2$  m. In the other, we assume that nothing is known about the source location so a uniform prior for the source location across the domain (250 m  $\times$  250 m) was assumed. In both cases, a uniform prior for the emission rate was assumed across the height domain (0–30 m).

For the Gaussian prior case, the CH<sub>4</sub> emission rate obtained using the Bayesian approach is  $Q = 7.52 \pm 2.23$  g/min (where the uncertainty is one standard deviation). This can be compared to the actual value of 5.80 g/min. Clearly the model overestimates the emission rate, but the actual value lies within the modelled uncertainty. The estimated source position has moved from that specified in the Gaussian prior and is  $x_s = -28.8 \pm 3.0$  m,  $y_s = 14.9 \pm 3.4$  m,  $z_s = 0.57 \pm 0.14$  m. The actual source position is  $x_s = -22$  m,  $y_s = 21$  m, and the release height  $z_s = 0.3$  m above ground level. Fig. 14a shows the sampled points for the horizontal source location. Most of the sampled points are concentrated about 10–15 m south-west of the real source. The square shape of the distribution of the sample points is due to the finite spatial resolution ( $\Delta x = \Delta y = 5$  m) in the determination of the source-receptor matrix using the backward Lagrangian stochastic model. One cannot expect the precision in the localization of position of source to be better than the inherent discretisation uncertainty due to the finite cell sizes.

For the case with the uniform prior for the source position, the source estimates are  $Q = 5.22 \pm 2.05$  g/min,  $x_s = -12.6 \pm 7.7$  m,  $y_s = -7.1 \pm 10.1$  m,  $z_s = 2.8 \pm 1.4$  m. The emission rate estimate has improved significantly compared to the case with the Gaussian prior but the source position estimate has worsened considerably together

with much higher uncertainty. One reason for this inferior performance could be that there are just not enough observations to constrain both position and emission rate properly without specifying a better prior.

Fig. 14b shows the sampled points for the horizontal source location for the uniform prior case. The sampled points are much more widely distributed than is the case with the Gaussian prior. Some of the shift in the sample points to closer to the east Picarro may be to compensate for the higher predicted value of the source height.

### 3.2.5. Mobile tracer technique using acetylene

The LGR instrument was moved through the plume at various distances downwind of the source. Fig. 15 shows an example of one set of transects where the CH<sub>4</sub> and C<sub>2</sub>H<sub>2</sub> concentrations are plotted as a function of time. In this example, the transects were made over a period of about 20 min approximately 90 m downwind from the source; the maximum CH<sub>4</sub> enhancement was about 1.6 ppm and the C<sub>2</sub>H<sub>2</sub> peak was 0.076 ppm. The average wind speed during this set of traverses was slightly above 5 m s<sup>-1</sup>, although it was quite gusty.

The plume is clearly defined in each traverse although there is substantial variation in the width and concentration reflecting the chaotic nature of the plume over relatively short timeframes. Despite the variability, the CH<sub>4</sub> and C<sub>2</sub>H<sub>2</sub> were well mixed in the plume with the C<sub>2</sub>H<sub>2</sub> tracer tracking that of CH<sub>4</sub> very closely. Similar results were obtained for all of the other tracer experiments, even under the very light and variable winds prevailing at the beginning of the first day.

Correlation between the two gasses was still very good even at 200 m downwind, however, the concentrations were significantly lower. For CH<sub>4</sub>, the maximum enhancement at 200 m was about 0.4 ppm whereas for the C<sub>2</sub>H<sub>2</sub>, the enhancement was generally less than about 0.02 ppm (i.e. 20 ppb). Although this was still well within the instrument's operating range, the signal to noise ratio especially for the C<sub>2</sub>H<sub>2</sub> was somewhat higher than the measurements made at the closer distances.

Emission estimates were calculated from each CH<sub>4</sub>/C<sub>2</sub>H<sub>2</sub> data pair measured by the LGR instrument during each plume transect experiment. This usually yielded at least several hundred emission rate estimates that were then averaged for each transect. Despite the wide concentration range encountered during each experiment (Fig. 15) the relative standard deviation of the estimates for each transect was usually less than 6%.

Ten separate emission estimates were made over the two days of the experiment; the results are summarised in Table 6. Transects 1–7 were

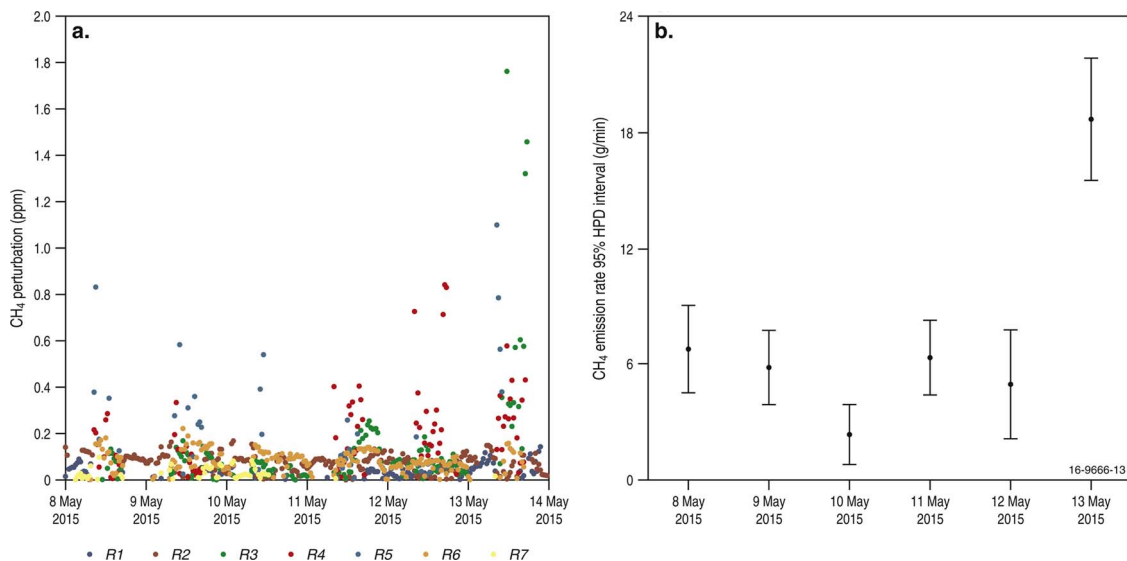


**Fig. 13.** Breakdown of daily emission rate estimates using the atmospheric tomography technique using the Boreal laser over the 8–13 May period. (a) background subtracted CH<sub>4</sub> average concentration for paths R1–R7 used in the Bayesian inversion (negative values removed) and (b) 95% emission rate interval for the rate estimate.



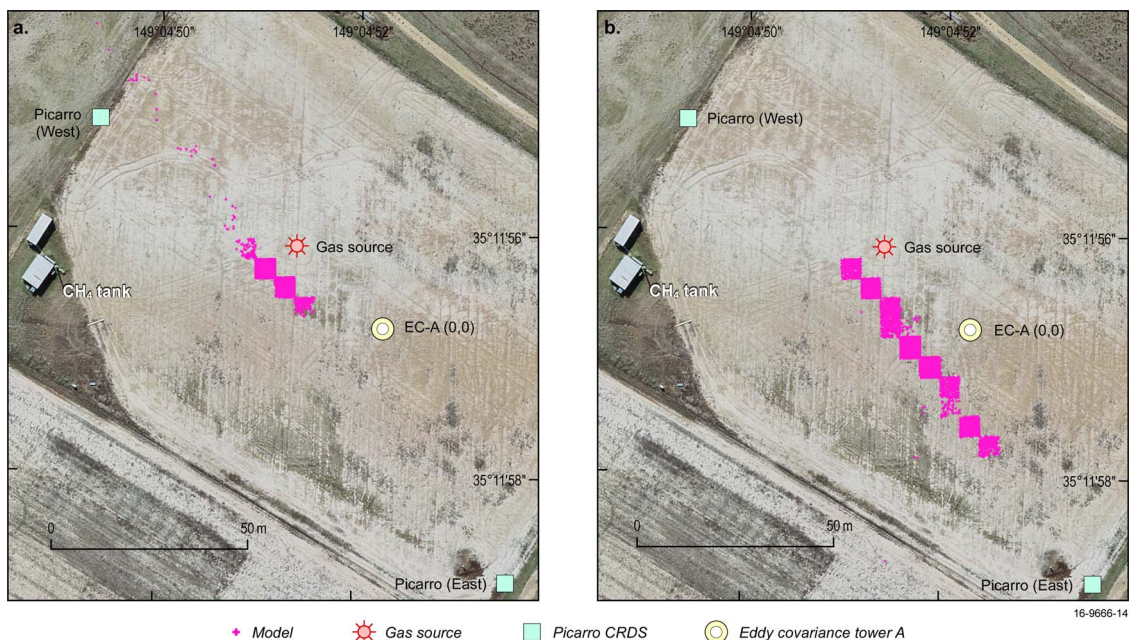


Fig. 14. Distribution of sample points for source location in the horizontal directions obtained from the MCMC sampling of the marginal bivariate posterior probability density function of the source parameters for CH<sub>4</sub> for (a) Gaussian source position prior, and (b) uniform source position prior. Eddy covariance tower A is the origin of the local coordinate system used in the modelling discussion.

made on 26 May while Transects 8–10 were made on 27 May. Transects 1 and 2 were made under very light wind conditions where the plume was ill defined and tended to move significantly during the experiments. Consequently, the LGR analyser was moved around the test range to locate the plume to record data. These transects are therefore made at various distances from the gas source; the

maximum concentrations shown in Table 6 were measured within about 5 m of the outlet. The other transects were made under more favourable wind conditions that produced a more defined plume and each transect was made roughly perpendicular to the wind direction across the plume.

The emission rate estimated for the standard flow rate was 5.9 g/

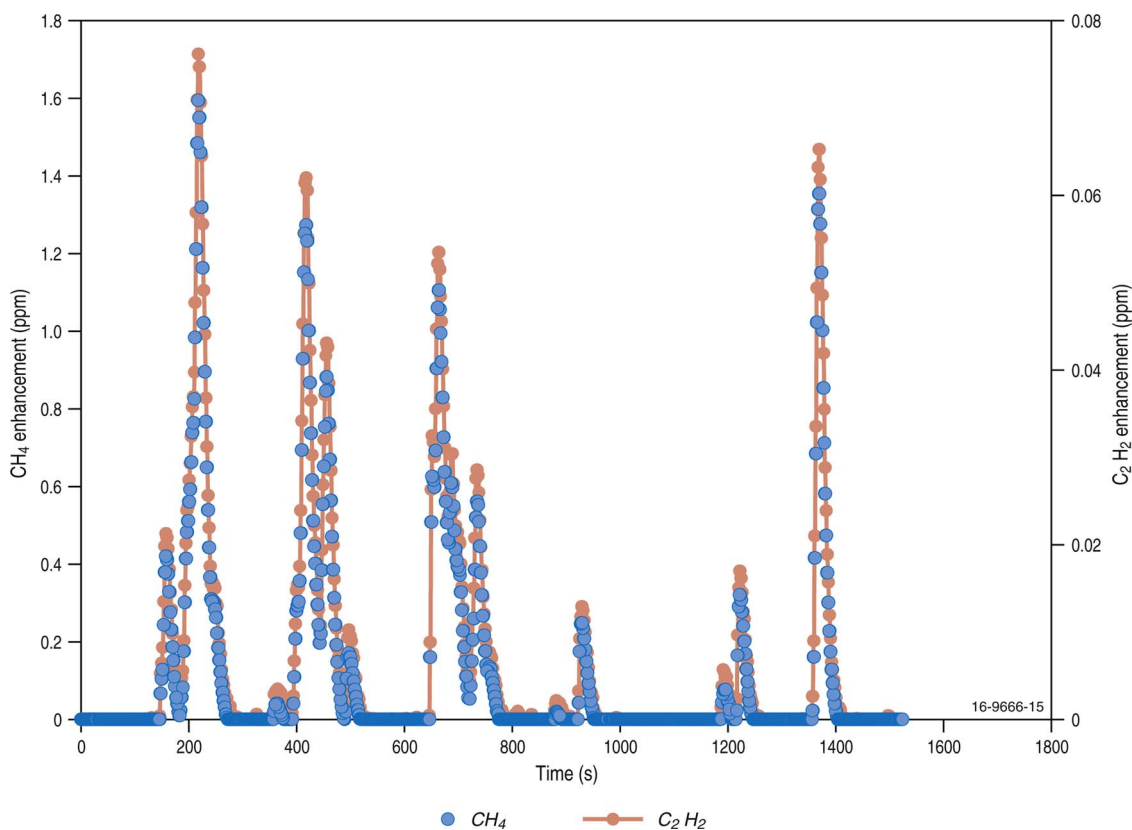


Fig. 15. Example of CH<sub>4</sub> and C<sub>2</sub>H<sub>2</sub> perturbation response and correlation during one of the traverses 90 m from the gas source using the LGR.

min during both Transects 1 and 2, which is within about 2% of the actual flow as measured by the mass flow controller (i.e. 5.8 g/min). The estimates for the other flow rates were also generally in good agreement with the actual flow, although at the highest flow rate of 20 g/min transects 8–10 underestimated the actual flow rate by approximately 12%.

### 3.2.6. Tracer technique using acetylene and canister measurements

Seven canister samples were collected over the two days; five were collected downwind in the plumes (Canisters 1–6) with the other two from upwind to provide background concentration data (Canisters 3 and 7). Subsequent analyses of the samples in the laboratory showed that the concentrations in one of the plume samples (Canister 5) were too close to the background to quantify, probably because the plume moved during the sampling period. Hence this sample was not used in the emission rate calculations. The emission rates estimated for CH<sub>4</sub> and CO<sub>2</sub> based on the canister samples are shown in Table 7.

The emission rates estimated by the canister samples showed significantly higher deviation from the nominal rates compared to those calculated from the online analyses provided by the LGR instrument. For CH<sub>4</sub> the estimates were between about 13 and 38% below the true emission rate. For CO<sub>2</sub>, agreement was better with estimates for Canisters 4 and 6 within 5% of the actual rate, although Canisters 1 and 2 showed higher variation. The overall average of the CO<sub>2</sub> results was 106 g/min, which was reasonably close to the actual rate of 100 g/min.

Some of the higher uncertainty of the canister estimates compared to those derived from the continuous measurements can be attributed to analytical uncertainty associated with the FTIR measurements, especially for the tracer which was present at low concentrations. Most of the canister samples had low concentrations initially but these were further diluted by the addition of nitrogen to pressurise the canister and this tended to reduce the precision of the results. For instance, variability in replicate analyses of the tracer alone could account for almost 10% uncertainty in the emission estimate. In addition, the emission estimate was sensitive to the background concentration (the  $B_{CH_4}$  and  $B_{Tracer}$  terms in Eq. (2)), especially as these varied significantly throughout the day.

The limited number of canister samples were collected for each transect contributed to the uncertainty in the emission estimates. Unlike the measurements made using the LGR instrument, where hundreds of individual measurements made over a period of about 20 min were used to derive an average emission rate, only a single canister was collected during each transect. The results in Table 7 show that in some individual cases, significant deviations from the nominal gas rates were estimated. However by averaging over a number of measurements, this error is reduced. For example in the case of CO<sub>2</sub> where four canister estimates were made, the average estimated emission rate was within about 6% of the true rate, despite some individual estimates differing by more than 25%.

**Table 6**

CH<sub>4</sub> rate estimates using the mobile acetylene tracer ratio technique using the LGR.

	Max CH <sub>4</sub> Concentration (ppm)	Max C <sub>2</sub> H <sub>2</sub> Concentration (ppm)	Downwind Distance (m)	Avg Wind Speed (m/s)	Estimated Rate (g/min)	Actual Rate (g/min)	Difference (%)
Transect 1	68.193	10.709	5 to 40	0.5	5.9 ± 0.30	5.8	1.9
Transect 2	78.357	12.595	5 to 40	1.1	5.9 ± 0.77	5.8	2.5
Transect 3	9.167	2.223	15	2.8	3.2 ± 0.17	2.9	9.7
Transect 4	25.447	2.414	15	2.7	8.8 ± 0.43	8.7	0.7
Transect 5	19.460	1.927	40	1.9	8.7 ± 0.23	8.7	-0.2
Transect 6	12.648	0.682	40	1.8	15.7 ± 0.46	16.4	-4.5
Transect 7	7.434	0.398	40	1.3	15.4 ± 0.55	16.4	-6.2
Transect 8	1.298	0.064	90	2.7	17.8 ± 0.74	20.0	-10.8
Transect 9	0.415	0.020	200	4.5	17.4 ± 0.51	20.0	-12.8
Transect 10	1.595	0.076	90	5.3	17.2 ± 0.60	20.0	-13.9

**Table 7**

Rate estimates for CO<sub>2</sub> and CH<sub>4</sub> using the acetylene tracer ratio technique and canister measurements.

	Canister 1	Canister 2	Canister 4	Canister 6
Downwind Distance (m)	< 5	10	40	40
Avg Wind Speed (m/s)	0.9	1	2.7	5.1
Concentration (ppm)				
CH <sub>4</sub>	92.38	2.853	2.956	5.015
CO <sub>2</sub>	1032.5	438.4	434.7	432.6
C <sub>2</sub> H <sub>2</sub>	17.96	0.159	0.125	0.187
Emission Rate (g/min)				
CH <sub>4</sub> estimated rate	4.3	5.1	7.3	14.5
CH <sub>4</sub> actual rate	5.8	5.8	8.7	20
Difference (%)	-33.7	-13.2	-19.4	-38.0
CO <sub>2</sub> estimated rate	79.6	138.5	103.6	102.0
CO <sub>2</sub> actual rate	100.0	100.0	100.0	100.0
Difference (%)	-25.7	27.8	3.5	2.0

### 3.2.7. Open-path FTIR spectrometer – WindTrax and tracer gas analysis

**3.2.7.1. Standard CH<sub>4</sub> flow rate.** Data were collected by the OP-FTIR instruments between 4 May and 6 June at the CH<sub>4</sub> standard release rate (5.8 g/min) and over 4 days (9–12 June) at the lower CH<sub>4</sub> release rate (5.0 g/min). Emission rates were retrieved from these data using 3 analysis techniques: bLS-Windtrax model, direct N<sub>2</sub>O tracer-gas technique, and Windtrax tracer-gas technique. At the standard release rate, the initial (blind) analysis returned emission estimates 17% and 14% higher than the actual release rate for the bLS-Windtrax model and direct N<sub>2</sub>O tracer-gas estimates, respectively.

As part of the final analysis several problems identified in these data were addressed. Both the emission estimate for CH<sub>4</sub> and N<sub>2</sub>O and the variability in the estimates were noted to increase in the second part of the measurement campaign. From the N<sub>2</sub>O retrieval by WindTrax, the daily average N<sub>2</sub>O emission rate varied from 0.66 to 1.23 g/min for a nominal release rate of 1.1 g/min. On several days slow decreases in measured release rate (relative to the measured CH<sub>4</sub> release rate) over the day (Supplementary information Fig. 14) or step changes (Supplementary information Fig. 15), coincident with interruptions or changes to the N<sub>2</sub>O or CH<sub>4</sub> release rates, were also noted (Please see Supplementary information R6 for a full description).

To limit any compromise of the N<sub>2</sub>O emission estimates, additional data filters were imposed on the tracer-gas analysis (See Supplementary information R6 for discussion):

- Minimum wind speed was increased from 1.5 to 2 m/s
- The background levels for N<sub>2</sub>O measured at upwind measurement paths differed by < 0.6 ppb
- Increase in N<sub>2</sub>O mixing ratio above background levels > 8 ppb
- Any decrease in the N<sub>2</sub>O emission rate, retrieved by WindTrax model, within a day was < 0.1 g/min

With these filters in place, the number of days when an emission rate for N<sub>2</sub>O tracer gas was retrieved from the WindTrax model was reduced to 16 days (4 May and 6 June 2015), compared with 27 days for CH<sub>4</sub>, with a higher proportion of days excluded from the later measurement period. The average emission rate for the 16 days was  $1.05 \pm 0.16$  g/min ( $n = 16$ ), with the variability in the emission estimates increased towards the end of the 4 week measurement period (initial 11 days  $1.06 \pm 0.05$  g/min ( $n = 8$ ) and  $1.05 \pm 0.23$  g/min for the final 11 days ( $n = 8$ )).

The estimated CH<sub>4</sub> release rate, and the variability in those estimates, derived from the three analysis methods (Windtrax, WindTrax-tracer and Direct Tracer-gas), increased over the 4 weeks of the measurements (Fig. 16). The CH<sub>4</sub> emission rate retrieved by WindTrax analysis, increased from  $6.04 \pm 0.29$  g/min for the initial measurements (4–14 May) to  $6.86 \pm 0.75$  g/min for the later period (19 May–6 June, release rate 5.8 g/min). While the emission rate estimated over the initial 10 days was 4.1% above the nominated release rate, the estimate for the final 10 days was 23.1% above the release rate, and the average emission estimate for the 4 weeks was 11.2% above the actual value (Table 7, Fig. 16). Using the tracer-gas to correct for errors in the model, the corresponding average CH<sub>4</sub> emission rate from the WindTrax-tracer ratio was within 8.9% of the release rate for the initial 10 days and 13.1% for the final 10 days, while the direct tracer-ratio analysis returned corresponding emission estimates within 3.8% (initial 10 days) and 11.9% (final 10 days) of the release rate.

The updated results reported here (Tables 2 and 7) for the standard CH<sub>4</sub> flow rate are derived from measurements in the initial 10 days of the trial (4–14 May 2015), due to this high uncertainty in the estimated

emissions during the latter part of the trial. Emission estimates for the full (4 May–6 June) and later (19 May–6 June) measurement periods are included in Table 7 for comparison.

The increase in the retrieved emission rate and corresponding increasing variability over the measurement period (release rate 5.8 g/min) is difficult to explain. Meteorological conditions were more favourable during the initial part of the measurements, with poor meteorological conditions (wind speeds between 1.5 and 2.5 m/s when gas was released) for 5% of the time, compared with 31% between 19 May and 6 June. The reported uncertainty in WindTrax retrieved emissions is typically 10% (Harper et al. 2010), with the variability in the emission rates retrieved by the WindTrax model noted to increase with increasing atmospheric stability. High emission estimates are also often associated with increasing atmospheric stability. However an analysis of the emission estimates with meteorological conditions indicate that wind speed, wind direction or differences between the measurement paths cannot account for the noted increase in emission estimates and uncertainties (See Supplementary information R6 for full analysis).

**3.2.7.2. Decreased CH<sub>4</sub> flow rate.** For the final 4 days of data collection, with a reduced CH<sub>4</sub> release rate (5.0 g/min; 9–12 June), the wind speed data filter was reduced to 1.5 m/s for the WindTrax based retrievals and 1.0 m/s for the direct tracer-gas retrievals to retain maximum data, as the stability of the retrieved N<sub>2</sub>O emission estimates had improved.

The retrieved CH<sub>4</sub> emission rate from the WindTrax-tracer analysis was within 0.5% of the nominated release rate. The direct tracer-gas analysis resulted in a lower average emission rate, within 2.3% of the release rate. While the results from the WindTrax-tracer and direct-

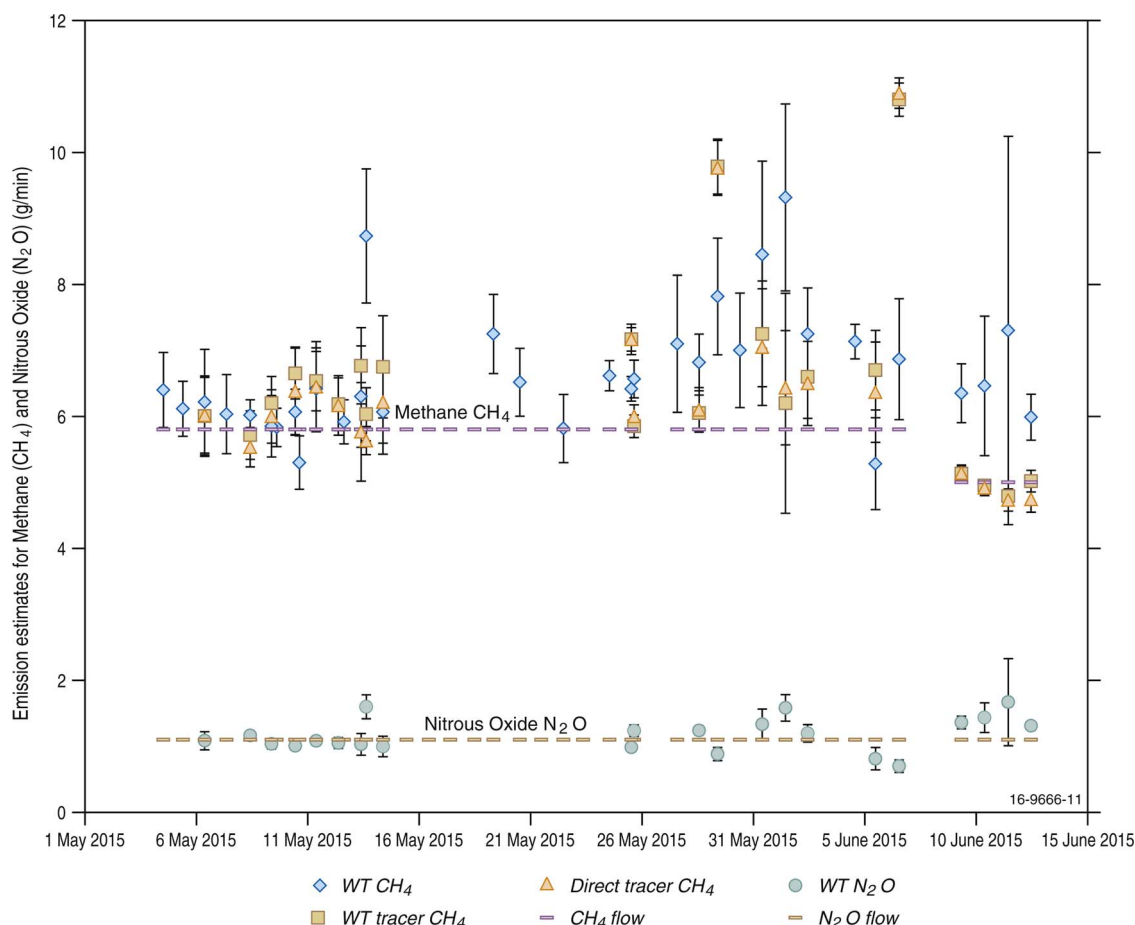


Fig. 16. Daily average CH<sub>4</sub> and N<sub>2</sub>O emission estimates calculated from OP-FTIR mixing ratio data using WindTrax, WindTrax-tracer gas ratio and direct tracer-gas ratio analysis, when the CH<sub>4</sub> and N<sub>2</sub>O were released at the standard rates (5.8 g/min and 1.1 g/min respectively). The CH<sub>4</sub> release rate was reduced to 5.0 g/min over 9–12 June. The error bars are 1 stdev of the average.

tracer analysis were similar, the inclusion of data collected when the wind speed was 1–1.5 m/s resulted in greater uncertainty in the emission estimates from the direct tracer-gas analysis (Supplementary information Figs. S18 and S19). In contrast the CH<sub>4</sub> and N<sub>2</sub>O emission rate retrieved from the WindTrax model was 30.5% and 31.3% respectively above the nominated release rate (Table 8, Supplementary information Fig. 19). The use of the tracer-gas in the analysis reduced the error in the emission estimates and also substantially reduced the variability in those estimates, from 9 and 10% for the CH<sub>4</sub> and N<sub>2</sub>O WindTrax retrieved estimates respectively, to 2.8% for CH<sub>4</sub> for the WindTrax-tracer and 3.9% for the direct tracer-gas analysis (Supplementary information Fig. S18).

Again for the final 4 days of measurement the very high emission rates retrieved by the WindTrax model cannot be explained by differences in wind speed, direction or varying upwind measurement paths. A comparison of the emission estimates with wind speed indicated that while the variability in emission estimates increased with decreasing wind speed (Supplementary information Fig. S19 OP-FTIR 6), there was no indication that increased emission estimates was influenced by wind speeds. Similarly there was no evidence that increased estimates was associated with wind direction (Supplementary information Fig. S20) or the measurement path employed (Supplementary information Fig. 21).

**3.2.7.3. CO<sub>2</sub> flow rate.** Meaningful results for the analysis of the CO<sub>2</sub> data were only available at the high release rate (300 g/min, 9–12 June 2015). At this higher rate, the increase in CO<sub>2</sub> was only 3–6 ppm above a background that varied by 0.5–2 ppm. While the data showed high uncertainty, the average emission estimate of 298 ± 101 g/min (WindTrax-tracer analysis) was within <1% of the actual release rate, while the WindTrax analysis returned an emission rate 25% greater than the release rate (Table 9; Supplementary information Fig. S22).

### 3.2.8. Gaussian plume fitting to mobile traverses

The LGR instrument on the (Husky) rover does not measure CO<sub>2</sub> but the Zebgas (Dynamet) sensor mounted on the rover provided concurrent CO<sub>2</sub> concentration data. During the run there were three passes that crossed the entire plume at about 90° to the wind direction. Emission rate estimates for CH<sub>4</sub> and CO<sub>2</sub> were calculated using these traverses. The measured CH<sub>4</sub> concentration for these three traverses and location of each traverse relative to the emission source is shown in Fig. 17. Similar profiles across each traverse were observed for CO<sub>2</sub> which was expected given the CO<sub>2</sub> and methane were released at the same location. However, there were some minor differences which reflect the differing responses of the two analysers and perhaps incomplete mixing of the CH<sub>4</sub> and CO<sub>2</sub> within the plume over the short

downwind fetch. A slight temporal offset was observed between the two gas profiles due to the delayed response time of the LGR compared to the Zebgas (Dyanmet) sensor (c.f. Figs. 8 and 9).

The three traverses were made at slightly different downwind distances between 13 and 16 m from the emission source. Note that although the emission rate was constant throughout the experiment, the CH<sub>4</sub> concentration varied significantly, which illustrates the short-term variability that typically occurs with plume measurements. This was especially the case in light winds such as those prevailing during these traverses ( $u \ll 1.5$  m/s). The plume data collected during the three traverses yielded CH<sub>4</sub> emission rates as shown in Table 10.

The average estimated CH<sub>4</sub> and CO<sub>2</sub> emission fluxes were 10.2 and 459 g/min, respectively. However, there was substantial variation between the individual traverse results, and given that there were only 3 traverses, the 95% confidence intervals for each estimate were quite wide; 10.2 ± 7.4 g/min for CH<sub>4</sub> and 459 ± 153 g/min for CO<sub>2</sub>. The actual release rates of methane and CO<sub>2</sub> were 20 g/min and 300 g/min respectively.

## 4. Conclusions and recommendations

The closest individual CH<sub>4</sub> rate estimate during the blind release experiment was within 2% of the actual release rate and was achieved using the acetylene tracer ratio technique. This quantification method also takes the least amount of time (i.e. a few hours) and does not require integrating the measurements with dispersion modelling. It appears to be highly suitable for obtaining an accurate measure of the emission for a single point in time, if the emission rate is relatively constant. If the emission rate varies significantly over time, then it would be necessary to make more frequent measurements to average temporal variations. Additionally, a tracer would need to be released continuously with the source while continuous downwind concentration measurements were made. Although this may be viable over shorter periods, it may not be practical over extended periods. For emission rates that vary over time (e.g. hour, daily, monthly), the other techniques deployed in this study appear suitable and can provide a good estimate of the average release rate.

The EC towers have the advantage of being completely solar powered and requiring very little maintenance or recalibration. They can be left for weeks unattended. EC data processing is the most laborious of all the techniques employed but optimised data filtering can provide a very accurate estimate of the release rate. The EC-FLS technique had one of the largest confidence interval ranges in its quantification estimate. This is due to a small sample set as towers C and D were installed later in the experiment and the coupling to the forward Lagrangian

**Table 8**

Average CH<sub>4</sub> emission rate (± 1 stdev) retrieved from OP-FTIR mixing ratio collected over 4 weeks and analysed using WindTrax model, WindTrax + tracer gas, and direct tracer-gas techniques once the emission rate was known. Included is the WindTrax analysis for the N<sub>2</sub>O emission rate.

	WindTrax		WT-Tracer	Direct tracer-gas
	CH <sub>4</sub> (g/min ± 1 stdev)	N <sub>2</sub> O (g/min ± 1 stdev)	CH <sub>4</sub> (g/min ± 1 stdev)	CH <sub>4</sub> (g/min ± 1 stdev)
Standard release rate 5.8 g/min CH <sub>4</sub> and 1.1 g/min N <sub>2</sub> O				
4–14 May 2015				
Average g/min	6.04 ± 0.29	1.06 ± 0.05	6.31 ± 0.37	6.02 ± 0.32
No. Days	13	8	9	9
19 May–6 June 2016				
Average g/min	6.86 ± 0.75	1.05 ± 0.23	6.54 ± 0.55	6.51 ± 0.44
No. Days	15	8	7	7
All: 4 May–6 June 2015				
Average g/min	6.48 ± 0.71	1.05 ± 0.16	6.41 ± 0.45	6.24 ± 0.45
No. Days	28	16	16	16
Low release rate 5.0 g/min CH <sub>4</sub> and 1.1 g/min N <sub>2</sub> O (9–12 June 2015)				
Average g/min	6.53 ± 0.56	1.44 ± 0.16	4.97 ± 0.14	4.88 ± 0.19
No. Days	4	4	4	4

**Table 9**  
Emission rate for CO<sub>2</sub> retrieved from OP-FTIR data collected between 9 and 12 June 2015, with analysis with the WindTrax model and WindTrax-tracer gas analysis. The actual CO<sub>2</sub> release rate was 300 g/min.

Date	CO <sub>2</sub> emissions (g/min ± 1 stdev) WindTrax	CO <sub>2</sub> emissions (g/min ± 1 stdev) WindTrax-tracer gas
9 June	447 ± 135	373 ± 70
10 June	257 ± 99	198 ± 51
11 June	473 ± 236	299 ± 54
12 June	278 ± 24	233 ± 23
9–12 June	376 ± 153	298 ± 101

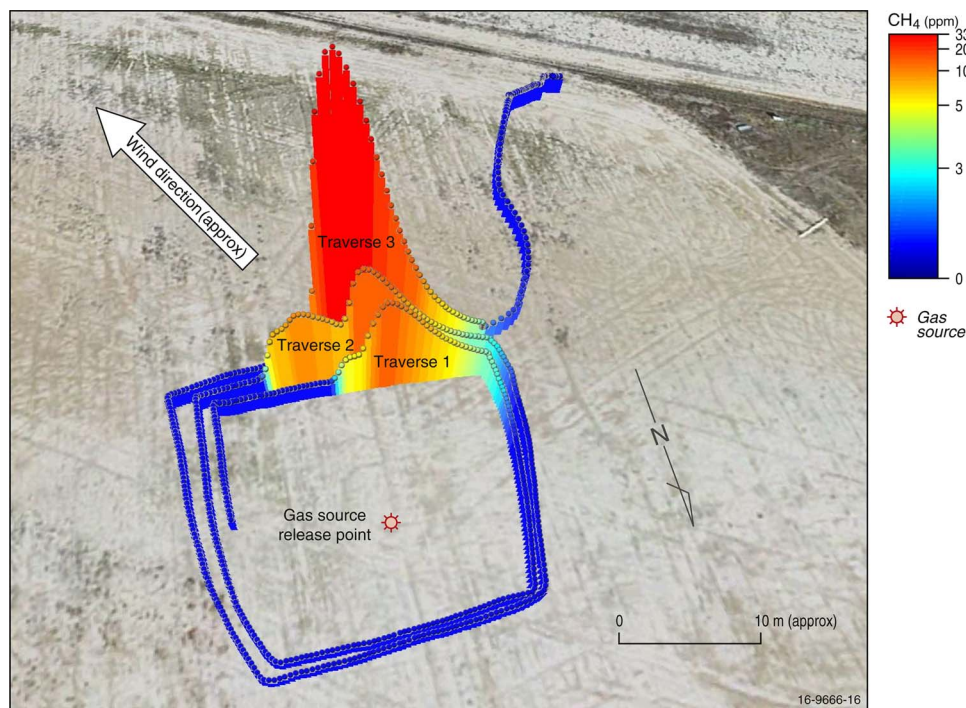


**Fig. 17.** Location and concentration of the methane plume measured with the LGR instrument during Husky runs. The peak of the traverses does not align with the wind direction due to the delayed rise time of the LGR instrument.

**Table 10**  
CO<sub>2</sub> and CH<sub>4</sub> rate estimates using data collected using the Husky ground robot.

Traverse	Downwind distance (m)	Average wind speed (m/s)	Maximum concentration perturbation (ppm)		Estimated emission rate (g/min)	
			CH <sub>4</sub> (LGR)	CO <sub>2</sub> (Dynamet)	CH <sub>4</sub>	CO <sub>2</sub>
1	13	1.3	10.6	306	4.7	343
2	14.5	1.2	13.0	245	8.3	425
3	16	1.1	30.8	367	17.4	608
				Average	10.2	459
				Actual rate	20.0	300

model requires cases where the point source and point tower measurement align. The EC-LS footprint model also has a point sensor and point source scenario, however the combined use of a footprint with the LS model provides an area proxy. If the emission source was an area opposed to a point source, it could be expected that EC coupled with a bLS model would produce a similar estimate compared to the FTIR-bLS, which, using a line sensor, was able to capture concentration over an area to better constrain plumes. A similar trend can be seen between the line and point based atmospheric tomography methods used, where the line method, which captures a concentration over an area, produced a more accurate emission rate although with similar confidence intervals. Line atmospheric tomography also demonstrated promise in being able

to respond to short term variations in the source emission rate, capturing a large sub- two hour emission spike while also capturing longer smaller shifts in emission rate.

Despite the seemingly scattered nature of the raw Boreal laser data, the data processing steps adopted in this study provided a useful dataset for the Bayesian inversions and could be used to derive a good estimate of the release rate. It appears data collected from continuous measurements over the course of a day provide better rate estimates than data from fewer but higher perturbation measurements. In contrast, too few perturbations above the background over the course of a day, and especially if limited to only one path, led to low emission estimates. Good practice would be to remove these low data periods from emission rate determinations.

Once the known emission rate was revealed, all techniques showed capability of producing accurate emission rates within 10% for the actual methane release rate. Improved plume modelling would decrease the uncertainty of many of the estimates. The results from this experiment highlight that which technique is best could depend on the situation, time allowed, and resources available. The study also illustrates the power of measuring the emission rate using multiple simultaneous methods and obtaining an ensemble median or mean. In the absence of any knowledge about a methane leak of critical importance, it is recommended that a minimum of three techniques be applied simultaneously and the results reported as the ensemble median and the uncertainty stated as the range of the method means.

It is worth re-emphasising that the techniques deployed for quantification of leakage in this study (i.e. once the location of a leak has

been identified) are unlikely to be effective for leak detection and localisation over large areas. That is a different challenge. UAVs equipped with higher precision and faster sensors than used in this study offer the potential to cover the large areas used for geological storage projects (1–10 km<sup>2</sup>) and detect isolated point sources of unusually elevated concentrations of CO<sub>2</sub> during normally well-mixed atmospheric daytime conditions. Being about to fly relatively slowly and have sensors within meters of the ground surface provides the ability for UAVs to detect much smaller leaks than would be possible using aircraft and satellite remote sensing techniques (Poppa, 2014) or using a fixed high-precision atmospheric monitoring station (Wilson et al., 2014). Any leakage from geological storage sites is likely to be highly localised (Feitz et al., 2014b) making mobile sensors an ideal platform for leakage detection. Detection of methane leaks is easier due to the lower atmospheric background concentration.

A hyperspectral imager's capacity to image the CH<sub>4</sub> release from 100 m, and a Boreal CH<sub>4</sub> laser sensor's ability to track moving targets suggest the future possibility to map gas plumes using a single laser and mobile aerial reflector. The Winsen CH<sub>4</sub> sensor in the Zebgas costs 10<sup>5</sup> times less than a LGR and is a fraction of its weight. While not equivalent in terms of performance, the sensitivity of miniaturised sensors is improving rapidly offering considerable potential for mobile applications, including automating gas monitoring and leak detection with mobile platforms such as ground robots or UAVs.

## Acknowledgements

We acknowledge funding provided by the Australian Government through the Carbon Capture and Storage – Implementation budget measure to support this research. The authors also acknowledge funding for the research provided by the Australian Government through the CRC program and support from the CO2CRC. The National Geosequestration Laboratory is thanked for making two Picarro instruments available for the study. We would like to thank Phil Dunbar and his staff (CSIRO Plant Industry) for maintaining the site and Dale Hughes (CSIRO) for his assistance with maintenance of the CSIRO EC tower. The authors also wish to acknowledge the assistance of Field Engineering Services at Geoscience Australia, Theo Chiotis for preparing the figures and Jacob Sohn (Geoscience Australia) for the carbon isotope measurements of the methane gas cylinder samples. Geoscience Australia and Western Sydney University team would like to acknowledge Charles Jenkins (CSIRO) for early discussions about the atmospheric tomography line technique and the Australian Mathematical Sciences Institute. The Macquarie University/University of Adelaide team wish to acknowledge financial support from the Environment Institute of The University of Adelaide, the Department of State Development of the Government of South Australia, Santos Pty Ltd, and the Australian Research Council (project LP140100460 and LP120200086). CSIRO Energy would like to acknowledge Mihaela Grigore for her assistance in development and calibration of the bench FTIR long path system. The University of Wollongong wishes to acknowledge Maximilien Desservetaz and Ruhi Humphries for their assistance in the site operations. The authors acknowledge the contributions from Andrew Bales and Armin Gembus from Bruker who provided the instrumentation and supported the acquisition of the Bruker HI90 data. AF and IS publish with the permission of the CEO, Geoscience Australia.

## Appendix A. Supplementary data

Supplementary data associated with this article can be found, in the online version, at <https://doi.org/10.1016/j.ijggc.2017.11.018>.

## References

Annan, J.D., Hargreaves, J.C., 2011. Understanding the CMIP3 multimodel ensemble. *J. Clim.* 24, 4529–4538.

- Baldocchi, D.D., 2003. Assessing the eddy covariance technique for evaluating carbon dioxide exchange rates of ecosystems: past, present and future. *Glob. Change Biol.* 9 (4), 479–492.
- Bhatia, S., Feitz, A., Francis, A., 2017. Atmospheric Tomography, GitHub Repository. <http://dx.doi.org/10.4225/25/5981136b54fe3>. [https://github.com/GeoscienceAustralia/atmospheric\\_tomography\\_laser](https://github.com/GeoscienceAustralia/atmospheric_tomography_laser).
- Bosse, M., Zlot, R., Flick, P., 2012. Zebdede: design of a spring-mounted 3-D range sensor with application to mobile mapping. *IEE Trans. Robot.* 28 (5), 1104–1119.
- Coates, T.W., Flesch, T.K., McGinn, S.M., Charmley, E., Chen, D., 2017. Evaluating an eddy covariance technique to estimate point-source emissions and its potential application to grazing cattle. *Agric. For. Meteorol.* 234–235, 164–171.
- Conley, S., Franco, G., Faloona, I., Blake, D.R., Peischl, J., Ryerson, T.B., 2016. Methane emissions from the 2015 Aliso Canyon blowout in Los Angeles, CA. *Science* 351 (6279), 1317–1320.
- Cossel, K.C., Waxman, E.M., Giorgetta, F.R., Cermak, M., Coddington, I.R., Hessesliu, D., Ruben, S., Swann, W.C., Truong, G.W., Rieker, G.B., Newbury, N.R., 2017. Open-path dual-comb spectroscopy to an airborne retroreflector. *Optica* 4, 724–728.
- Day, S., Dell'Amico, Fry, R., Javanmard Tousi, H., 2014. Field Measurements of Fugitive Emissions from Equipment and Well Casings in Australian Coal Seam Gas Production Facilities. CSIRO, Australia.
- Dixon, T., Romanak, K.D., 2015. Improving monitoring protocols for CO<sub>2</sub> geological storage with technical advances in CO<sub>2</sub> attribution monitoring. *Int. J. Greenh. Gas Control* 41, 29–40.
- Etheridge, D., Luhar, A., Loh, Z., Leuning, R., Spencer, D., Steele, P., Zegelin, S., Allison, C., Krummel, P., Leist, M., van der Schoot, M., 2011. Atmospheric monitoring of the CO<sub>2</sub>CRC Otway Project and lessons for large scale CO<sub>2</sub> storage projects. *Energy Procedia* 4, 3666–3675.
- Etheridge, D.M., Day, S., Hibberd, M.F., Luhar, A., Spencer, D.A., Loh, Z.M., Zegelin, S., Krummel, P.B., van Gorsel, E., Thornton, D.P., Gregory, R.L., Ong, C., Barrett, D., 2016. Characterisation of Regional Fluxes of Methane in the Surat Basin, Queensland–Milestone 3.1 GISERA Greenhouse Gas Research – Phase 3. CSIRO, Australia.
- Feitz, A., Jenkins, C., Schacht, U., McGrath, A., Henry, B., Schroder, I., Noble, R., Kuske, T., George, S., Charles, H., Zegelin, S., Cumow, S., Zhang, H., Sirault, X., Jimenez-Berni, J., Hortle, A., 2014a. An assessment of near surface CO<sub>2</sub> leakage detection techniques under Australian conditions. *Energy Procedia* 63, 3891–3906.
- Feitz, A.J., Leamon, G., Jenkins, C., Jones, D.G., Moreira, A., Bressan, L., Melo, C., Dobeck, L.M., Repasky, K., Spangler, L.H., 2014b. Looking for leakage or monitoring for public assurance? *Energy Procedia* 63, 3881–3890.
- Feitz, A.J., Schroder, I.F., Jenkins, C.J., Schacht, U., Zegelin, S., Berko, H., McGrath, A., Noble, R., Palu, T.J., George, S., Heath, C., Zhang, H., Sirault, X., Jimenez-Berni, J., 2016. Ginninderra Controlled CO<sub>2</sub> Release Facility Dataset 2012–2013. Geoscience Australia and CO<sub>2</sub>CRC, Canberra. <http://dx.doi.org/10.4225/25/5823c37333f9d>.
- Flesch, T.K., Wilson, J.D., Yee, E., 1995. Backward-time Lagrangian stochastic dispersion models and their application to estimate gaseous emissions. *J. Appl. Meteorol.* 34, 1320–1332.
- Flesch, T.K., Wilson, J.D., Harper, L.A., Crenna, B.P., Sharpe, R.R., 2004. Deducing ground-to-air emissions from observed trace gas concentrations: a field trial. *J. Appl. Meteorol.* 43, 487–502.
- Francey, R.J., Steele, L.P., Spencer, D.A., Langenfelds, R.L., Law, R.M., Krummel, P.B., Fraser, P.J., Etheridge, D.M., Derek, N., Coram, S.A., Cooper, L.N., Allison, C.E., Porter, L., Baly, S., 2003. The CSIRO (Australia) measurement of greenhouse gases in the global atmosphere. In: Toru, S., Kazuto, S. (Eds.), Report of the 11th WMO/IAEA Meeting of Experts on Carbon Dioxide Concentration and Related Tracer Measurement Techniques, Tokyo, Japan, September 2001. World Meteorological Organization Global Atmosphere Watch 97–111.
- Griffith, D.W.T., 1996. Synthetic calibration and quantitative analysis of gas-phase FT-IR spectra. *Appl. Spectrosc.* 50, 59–70.
- Hanna, S.R., Briggs, G.A., Hosker Jr, R.P., 1982. Handbook on Atmospheric Diffusion (No. DOE/TIC-11223). National Oceanic and Atmospheric Administration and Atmospheric Turbulence and Diffusion Lab, Oak Ridge, TN (USA).
- Harig, R., Matz, G., Rusch, P., Gerhard, J.H., Schaefer, K.P., Jahn, C., Schwengler, P., Beil, A., 2003. Remote detection of methane by infrared spectrometry for airborne pipeline surveillance: first results of ground-based measurements. *Proceedings of SPIE*, vol. 4539, 435–446.
- Harper, L.A., Flesch, T.K., Weaver, K.H., Wilson, J.D., 2010. The effect of biofuel production on swine farm methane and ammonia emissions. *J. Environ. Qual.* 39, 1984–1992.
- Hirst, B., 2012. A new approach to detecting, locating and quantifying surface gas fluxes above an onshore CO<sub>2</sub> storage project. In: Proceedings of the 11th Annual Conference on Carbon Capture Utilization & Sequestration. 29 April–3 May, 2012, Pittsburgh, Pennsylvania.
- Hirst, B., Randell, D., Jones, M., Jonathan, P., King, B., Dean, M., 2017. A new technique for monitoring the atmosphere above onshore carbon storage projects that can estimate the locations and mass emission rates of detected sources. *Energy Procedia* 114, 3716–3728.
- Humphries, R., Jenkins, C., Leuning, R., Zegelin, S., Griffith, D., Caldwell, C., Berko, H., Feitz, A., 2012. Atmospheric tomography: a Bayesian inversion technique for determining the rate and location of fugitive emissions. *Environ. Sci. Technol.* 46, 1739–1746.
- Jenkins, C.R., Cook, P.J., Ennis-King, J., Underschlutz, J., Boreham, C., Dance, T., de Caritat, P., Etheridge, D.M., Freifeld, B.M., Hortle, A., Kirste, D., Paterson, L., Pevzner, R., Schacht, U., Sharma, S., Stalker, L., Urosevic, M., 2012. Safe storage and effective monitoring of CO<sub>2</sub> in depleted gas fields. *Proc. Natl. Acad. Sci.* 109, E35–E41.
- Jenkins, C.R., Kuske, T., Zegelin, S., 2016. Simple and effective atmospheric monitoring

- for CO<sub>2</sub> leakage. *Int. J. Greenh. Gas Control* 46, 158–174.
- Jones, D.G., Barlow, T., Beaubien, S.E., Ciotoli, G., Lister, T.R., Lombardi, S., May, F., Möller, I., Pearce, J.M., Shaw, R.A., 2009. New and established techniques for surface gas monitoring at onshore CO<sub>2</sub> storage sites. *Energy Procedia* 1, 2127–2134.
- Kaul, L., Zlot, R., Bosse, M., 2016. Continuous-time three-dimensional mapping for micro aerial vehicles with a passively actuated rotating laser scanner. *J. Field Robot.* 33 (1), 103–132.
- Kuske, T., Jenkins, C., Zegelin, S., Mollah, M., Feitz, A., 2013. Atmospheric tomography as a tool for quantification of CO<sub>2</sub> emissions from potential surface leaks: signal processing workflow for a low accuracy sensor array. *Energy Procedia* 37, 4065–4076.
- Lambert, S.J., Boer, G.J., 2001. CMIP1 evaluation and intercomparison of coupled climate models. *Clim. Dyn.* 17, 83–106.
- Lewicki, J.L., Hilley, G.E., 2009. Eddy covariance mapping and quantification of surface CO<sub>2</sub> leakage fluxes. *Geophys. Res. Lett.* 36, L21802.
- Lewicki, J.L., Fischer, M.L., Hilley, G.E., 2008. Six-week time series of eddy covariance CO<sub>2</sub> flux at Mammoth Mountain, California: performance evaluation and role of meteorological forcing. *J. Volcanol. Geotherm. Res.* 171 (3), 178–190.
- Loh, Z.M., Leuning, R., Zegelin, S.J., Etheridge, D.M., Bai, M., Naylor, T., Griffith, D., 2009. Testing Lagrangian atmospheric dispersion modelling to monitor CO<sub>2</sub> and CH<sub>4</sub> leakage from Geosequestration. *Atmos. Environ.* 43, 2602–2611.
- Luhar, A.K., Etheridge, D.M., Leuning, R., Loh, Z.M., Jenkins, C.R., Yee, E., 2014. Locating and quantifying greenhouse gas emissions at a geological CO<sub>2</sub> storage site using atmospheric modeling and measurements. *J. Geophys. Res.: Atmos.* 119, 10959–10979.
- Mauder, M., Foken, T., 2004. Documentation and Instruction Manual of the Eddy Covariance Software Package TK2. Universität Bayreuth, Abt. Mikrometeorologie Arbeit sergebnisse 26, 44 pp. (Print: ISSN 1614-8916; Internet: ISSN 1614-8926).
- Mauder, M., Cuntz, M., Driue, C., Graf, A., Rebmann, C., Schmid, H.P., Schmidt, M., Steinbrecher, R., 2013. A strategy for quality and uncertainty assessment of long-term eddy-covariance measurements. *Agric. For. Meteorol.* 169, 122–135.
- Moncrieff, J.B., Massheder, J.M., De Bruin, H., Elbers, J., Friborg, T., Heusinkveld, B., Kabat, P., Scott, S., Søgaard, H., Verhoef, A., 1997. A system to measure surface fluxes of momentum, sensible heat, water vapour and carbon dioxide. *J. Hydrol.* 188, 589–611.
- Moncrieff, J., Clement, R., Finnigan, J., Meyers, T., 2005. Averaging, detrending, and filtering of eddy covariance time series. *Handbook of Micrometeorology*. Springer, Netherlands.
- Myers, J., Kelly, T., Lawrie, C., Riggs, K., 2000. Environmental Technology Verification Report: Boreal Laser Inc. GasFinder 2.0 Tunable Diode Laser Open Path Monitor. Battelle, Columbus.
- Nakai, T., Shimoyama, K., 2012. Ultrasonic anemometer angle of attack errors under turbulent conditions. *Agric. For. Meteorol.* 162, 14–26.
- Omara, M., Sullivan, M.R., Xiang Li Subramanian, R., Robinson, A.L., Presto, A.A., 2016. Methane emissions from conventional and unconventional natural gas production sites in the Marcellus shale basin. *Environ. Sci. Technol.* 50, 2099–2107.
- Poppa, F., 2014. Towards UAV-Assisted Monitoring of Onshore Geological CO<sub>2</sub> Storage Sites. Australian National University, Canberra PhD Thesis.
- Quigley, M., Conley, K., Gerkey, B.P., Faust, J., Foote, T., Leibs, J., Wheeler, R., Ng, A.Y., 2009. ROS: an open-source Robot Operating System. *ICRA Workshop on Open Source Software* vol. 5, no. 3.2, 5 pp.
- Ro, K.S., Johnson, M.H., Hunt, P.G., Flesch, T.K., 2011. Measuring trace gas emission from multi-distributed sources using vertical radial plume mapping (VRPM) and backward Lagrangian stochastic (bLS) techniques. *Atmosphere* 2, 553–566.
- Rothman, L.S., Gordon, I.E., Barbe, A., Benner, D.C., Bernath, P.F., Birk, M., Boudon, V., Brown, L.R., Campargue, A., Champion, J.P., Chance, K., Coudert, L.H., Dana, V., Devi, V.M., Fally, S., Flaud, J.M., Gamache, R.R., Goldman, A., Jacquemart, D., Kleiner, I., Lacombe, N., Lafferty, W.J., Mandin, J.Y., Massie, S.T., Mikhailenko, S.N., Miller, C.E., Moazzen-Ahmadi, N., Naumenko, O.V., Nikitin, A.V., Orphal, J., Perevalov, V.I., Perrin, A., Predoi-Cross, A., Rinsland, C.P., Rotger, M., Šimečková, M., Smith, M.A.H., Sung, K., Tashkun, S.A., Tennyson, J., Toth, R.A., Vandaele, A.C., Vander Auwera, J., 2009. The HITRAN 2008 molecular spectroscopic database. *J. Quant. Spectrosc. Radiat. Transf.* 110, 533–572.
- Thomson, D.J., 1987. Criteria for the selection of stochastic models of particle trajectories in turbulent flows. *J. Fluid Mech.* 180, 529–556.
- Thunder Beach Scientific, 2013. Windtrax, version 2.0.8.1. Thunder Beach Scientific, Nanaimo, Canada. <http://www.thunderbeachscientific.com/>.
- Toth, Z., Talagrand, O., Candille, G., Zhu, Y., 2003. Probability and ensemble forecasts. *Forecast Verification: A Practitioners Guide in Atmospheric Science*. pp. 137–163.
- United Nations Framework Convention on Climate Change, 2015. INDCs as Communicated by Parties. <http://www4.unfccc.int/submissions/indc/Submission%20Pages/submissions.aspx>.
- van Leeuwen, C., Hensen, A., Meijer, H.A.J., 2013. Leak detection of CO<sub>2</sub> pipelines with simple atmospheric CO<sub>2</sub> sensors for carbon capture and storage. *Int. J. Greenh. Gas Control* 19, 420–431.
- Vickers, D., Mahrt, L., 1997. Quality control and flux sampling problems for tower and aircraft data. *J. Atmos. Ocean. Technol.* 14, 512–526.
- Webb, E.K., Pearman, G.I., Leuning, R., 1980. Correction of flux measurements for density effects due to heat and water vapour transfer. *Q. J. R. Meteorol. Soc.* 106, 85–100.
- Werner, C., Chiodini, G., Voigt, D., Caliro, S., Avino, R., Russo, M., Brombach, T., Wyngaard, J., Brantley, S., 2003. Monitoring volcanic hazard using eddy covariance at Solfatara volcano, Naples, Italy. *Earth Planet. Sci. Lett.* 210 (3), 561–577.
- Wilks, 1995. *Statistical Methods in the Atmospheric Sciences*. Vol 59 of International Geophysics Series. Academic Press, London.
- Wilson, J.D., Sawford, B.L., 1996. Review of Lagrangian stochastic models for trajectories in the turbulent atmosphere. *Bound. Layer Meteorol.* 78, 191–210.
- Wilson, P., Feitz, A., Jenkins, C., Berko, H., Loh, Z., Luhar, A., Hibberd, M., Spencer, D., Etheridge, D., 2014. Sensitivity of CO<sub>2</sub> leak detection using a single atmospheric station. *Energy Procedia* 63, 3907–3914.
- Zazzeri, G., Lowry, D., Fisher, R.E., France, J.L., Lanoisellé, M., Nisbet, E.G., 2015. Plume mapping and isotopic characterisation of anthropogenic methane sources. *Atmos. Environ.* 11, 151–162.